Engineering Failure Analysis 156 (2024) 107758

Contents lists available at ScienceDirect

Engineering Failure Analysis

journal homepage: www.elsevier.com/locate/engfailanal

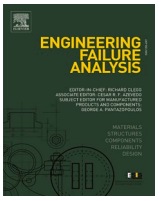

Failure analysis and electrochemical testing of ammonium chloride corrosion in a heat exchanger in a diesel hydrotreating unit of a petroleum refinery

Jancler Adriano Pereira Nicacio [a,*], Fernando Castro Oliveira [b], Marcello Rosa Dumont [a]

[a] Federal Center for Technological Education of Minas Gerais, Belo Horizonte-MG 30421169, Brazil
[b] Federal Center for Technological Education of Minas Gerais, Timóteo-MG 35180008, Brazil

ARTICLE INFO

Keywords:
Ammonium chloride
NH_4Cl corrosion
Austenitic stainless steels
Heat exchanger
Electrochemical corrosion tests

ABSTRACT

Crude oil is a complex mixture of hydrocarbons and can contain various impurities, which vary depending on the source and geographical location from which it is extracted. These impurities include sulphur, nitrogen, some metals, asphaltenes, non-condensable gases and salts. Salts in oil are typically found in the form of ions, which means that they are dissolved in the water present in the crude oil, or in the form of solid salts that are later deposited in equipment, pipes, and ducts. These salts can be harmful because, when the oil is processed, the water present in the oil can separate from the hydrocarbons and cause corrosion of equipment in the oil refining plant. In addition, salts can form solid deposits that can obstruct equipment. It is therefore important to remove or reduce the presence of salts in oil during the refining process to avoid operational problems and problems with the quality of the refined product. Several occurrences are reported in the specialized literature of equipment failures in the oil refining industry involving corrosion by salts, especially ammonium chloride salts. Basically, ammonium chloride, whose chemical formula is NH_4Cl, is an inorganic chemical compound consisting of ammonium ions ($NH4^{+}$) and chloride ions (Cl^{-}), It is known by several names, including "ammonium salt" or "ammonium salt" due to its composition. The aim of this paper is to investigate the failure of a shell-and-tube heat exchanger in the charge preheater system of the diesel hydrotreating unit of a Brazilian oil refinery, in which the root cause of the failure identified as responsible for the damage was ammonium chloride corrosion. A severe corrosive process was observed in the tubes of the tube bundle, including perforation in some tubes, as well as damage to the inside of the heat exchanger shell. The analysis methods employed involved the study of three different types of austenitic stainless steel in terms of corrosion resistance: 304, 316L and 317L, which were exposed to media containing sodium chloride and ammonium chloride at a concentration of 3.5 % (m/v). Two electrochemical corrosion tests were carried out in aqueous media, the first determining potentiodynamic polarization curves and the second electrochemical impedance spectroscopy. In addition to material characterization tests, such as determining the chemical composition, hardness and scanning electron microscopy of the corroded samples. The results of this paper indicate that the 317L steel samples have larger passivation regions, higher pitting potential values, lower passivation current density values, as well as lower corrosion rate values during the simulation of the equivalent electrochemical circuit, which implies greater resistance to corrosion

* Corresponding author.
E-mail address: jancler@petrobras.com.br (J.A. Pereira Nicacio).

https://doi.org/10.1016/j.engfailanal.2023.107758
Received 13 July 2023; Received in revised form 25 October 2023; Accepted 29 October 2023
Available online 10 November 2023

in a medium containing ammonium chloride, compared to the others. The conclusions reached reveal the applicability of 317L austenitic stainless steel in environments containing ammonium chloride, such as in the diesel hydrotreating sections of oil refineries, in addition to the use of washing water in pipes and equipment to dissolve these salts. Due to the high corrosion resistance of 317L steel in media containing ammonium chloride, it could be extended to other refining sections, such as distillation, cracking and coking units in oil refineries. This research will enable potential gains in terms of increasing the operational life of equipment and installations, reducing corrective maintenance interventions and operational safety in the operation of the industrial plant.

1. Introduction

The hydrotreating process is widely used to remove contaminants in petroleum fractions to adapt them to the specifications of commercial products. In diesel fuel, it aims to remove sulfur and nitrogen from sulfur and nitrogen compounds naturally present in the distillate fractions of petroleum or resulting from the processing of fractions in intermediate conversion units [1–6]. In general, in oil refineries, hydrotreating units operate at pressures between 30 kgf cm^{-2} and 200 kgf cm^{-2} and temperatures of approximately 250 °C to 450 °C, in which design pressure and temperature are defined according to the nature of the load and required conversion [7–10]. After the discovery of extensive oil exploration fields in the so-called pre-salt layer off the Brazilian coast, and its commercial exploitation, it is clear due to the oil loads currently processed in Brazilian refineries, there is a recurrence of problems related to ammonium chloride salt corrosion (NH_4Cl) in hydrotreating units [11–13]. Its formation occurs by the reaction of ammonia (NH_3) with hydrochloric acid (HCl), both in the vapor phase, crystallizing and forming the salt. The presence of this salt produces a highly aggressive form of localized corrosion. Some evident failures occurred in effluent systems from hydrotreating reactors due to ammonium salt corrosion [14–18].

Austenitic stainless steels are generally resistant to corrosion in many environments but can be affected by stress corrosion and localized corrosion in the presence of chlorides, such as ammonium chloride salt [19–21]. Stress corrosion is a type of corrosion that occurs under mechanical stress in combination with the presence of chloride ions. Localized corrosion includes pitting and intergranular corrosion. Pitting corrosion is a type of localized corrosion that can occur in austenitic stainless steels in the presence of chlorides [22–25]. It involves the formation of small cavities or “pits” on the surface of the material, which can be particularly problematic as the cavities can expand rapidly. The ammonium chloride salt, if present, can provide the chloride ions needed to initiate pitting corrosion [26]. Pitting corrosion is problematic because, even if most of the metal surface remains apparently intact, the presence of pitting can weaken the material and lead to premature failure. To prevent or minimize pitting corrosion, it is important to choose corrosion-resistant materials, protect metal surfaces with appropriate coatings and avoid corrosive environments whenever possible [27–30].

This objective of study addresses an investigation of the failure mechanisms carried out in a heat exchanger shell and tubes of a diesel hydrotreating unit in a Brazilian refinery, where it was found that ammonium chloride corrosion was the root cause of the observed damage. The equipment, the object of the failure analysis, which took place in the first half of 2022, was the load pre-heater heat exchanger of the diesel hydrotreating unit E-0004 and on the sides of the tubes it operates with effluent from the reactor R-0001of the hydrotreating unit (Hydrocarbons + H_2 + H_2S), and on the shell side it operates with petcoke and direct distillation diesel (1470 $m^3.day^{-1}$ and 2030 $m^3.day^{-1}$). The exchanger has a design pressure of 116 $kgf.cm^{-2}$ for the shell and 99 $kgf.cm^{-2}$ for the beam and an operating pressure of 99.6 $kgf.cm^{-2}$ for the shell and 84.9 $kgf.cm^{-2}$. It has a design temperature of 252 °C for the shell and 319 °C for the beam and an operating temperature of 134 °C for the shell and 390 °C for the beam, it should be noted that the equipment does not work above the design temperature. It presents a total thermal load of 2.22 $Mkcal.h^{-1}$. The shell is 7.50 m long and has an internal diameter of 1.25 m, a wall thickness of 12.5 mm produced in low alloy carbon steel, the tube bundle has 212 tubes and a diameter of 19.05 mm, and wall thickness of 2.11 mm produced in low alloy carbon of ASTM A213 Tp. 304 specification, a specific steel for heat exchange tubes. The unit’s current load is around 3500 $m3.day^{-1}$.

The unit started working in 2004 and the failure was observed in the first half of 2022, with an expected operational lifetime of the unit of around 50 years. In the first phase of the study, the investigation of the failure that occurred in the heat exchanger was addressed, where non-destructive thickness testing by ultrasound was carried out on the exchanger shell. The eddy current test in the tubes of the exchanger beam was carried out to verify the thickness loss. The residues found in the heat exchanger (products corrosion) were analyzed and their chemical composition was determined, showing evidence of the presence of ammonium chloride salts. In the second phase, electrochemical tests of potentiodynamic polarization and electrochemical impedance spectroscopy were conducted to determine the corrosion resistance in a medium containing ammonium chloride of three different austenitic stainless steels, 304, 316L and 317L, thus showing more resistant material for applications on the heat exchanger shell and tube bundle.

2. Theory

2.1. Diesel hydrotreatment process

The reactions that occur in a hydrotreating process are predominantly exothermic, therefore, releasing heat. In many cases,

depending on the amount and type of contaminating compounds and the severity of the process, some catalyst beds need to be used between them, to control the evolution of the reactor thermal profile [31]. By process severity, we mean the operational conditions to which an industrial unit is submitted, such as high values of pressure, temperature, vibration, friction, exposure to corrosive agents [32]. Although it is complex to accurately exemplify the chemical reactions that occur in the hydrotreatment process, due to the wide range of existing compounds, we can cite the hydrodesulphurization, hydrogenation and hydrodenitrogenation reactions [33,34].

In hydrodesulfurization reactions, sulfur compounds in oil, mercaptans, sulfides and disulfides, are easily hydrogenated. On the other hand, aromatic sulfides require more severe hydrotreating conditions. This reaction is strongly influenced by temperature and velocity [35].

Hydrogenation reactions are thermodynamically favored under the usual hydrofining conditions and their rates are quite high. Therefore, the hydrogenations of monolefins and diolefins, in general, are not limiting in processes where the main aim is to remove sulfur and nitrogen [36]. Hydrodenitrogenation reactions are slower than desulfurization reactions. Compounds containing non-heterocyclic nitrogen (aliphatic amines and nitriles) are easier to react than ring nitrogen compounds. However, these compounds are generally found at a lower concentration in petroleum fractions [37,38].

Fig. 1 shows the schematic flowchart of the diesel hydrotreating unit, where the failure analysis in this work occurred. K (compressor), E (heat exchanger), F (furnace), R (reactor) and V (pressure vessel) are shown, the arrows indicate the flow direction inside the processing unit.

2.2. The formation of ammonium chloride

Ammonium chloride (NH_4Cl) is a type of salt formed in the high-pressure section of hydrotreating units and is associated with the contaminants in the load [39]. In general, the formation of ammonium chloride is observed for chloride concentrations above 2.0 wt% [40].

The loads of these units present chloride and nitrogen compounds, which react with hydrogen forming hydrochloric acid (HCl) and ammonia (NH_3), respectively. Additives used in oil streams as neutralizers can add traces of nitrogenous compounds to the load [41].

All metallic materials commonly used in oil refineries are susceptible to attack by ammonium chloride, such as carbon steel, low alloy steel, stainless steel, duplex steel, nickel–iron-chromium based alloys (Incoloy) 800 and 825, nickel-based alloys (Inconel) 625 and nickel–chromium-molybdenum-based alloys (Hastelloy) 276 and titanium [42]. Ammonium chloride is an ionic compound formed by the combination of an acid (hydrochloric acid) and a base (ammonia). Although ammonium chloride can be corrosive under certain conditions, its corrosive action is generally considered to be less intense compared to pure HCl, corrosion caused by ammonium chloride tends to be milder and less aggressive [43]. The formation of the ammonium chloride salt, Equation (1), comes from the hydrodenitrogenation reactions in the reaction section of the hydrotreating units with chloride ions [44].

$$NH_{3(g)} + HCl_{(g)} \rightarrow NH_4Cl_{(s)} \quad (1)$$

The process variables that influence the formation of ammonium chloride are concentration/partial pressure of contaminants and temperature. Regarding the concentration of contaminants, this is a function of the content of contaminants in the load and the severity of the hydrotreatment process (the greater the severity, the greater the concentration of HCl and NH_3) [45].

The Equation (2) involves solid ammonium chloride being dissolved in water to form ammonium ions and chloride ions. When ammonium chloride is dissolved in water, the ionic bonds that hold the ammonium and chloride ions together in the solid are broken,

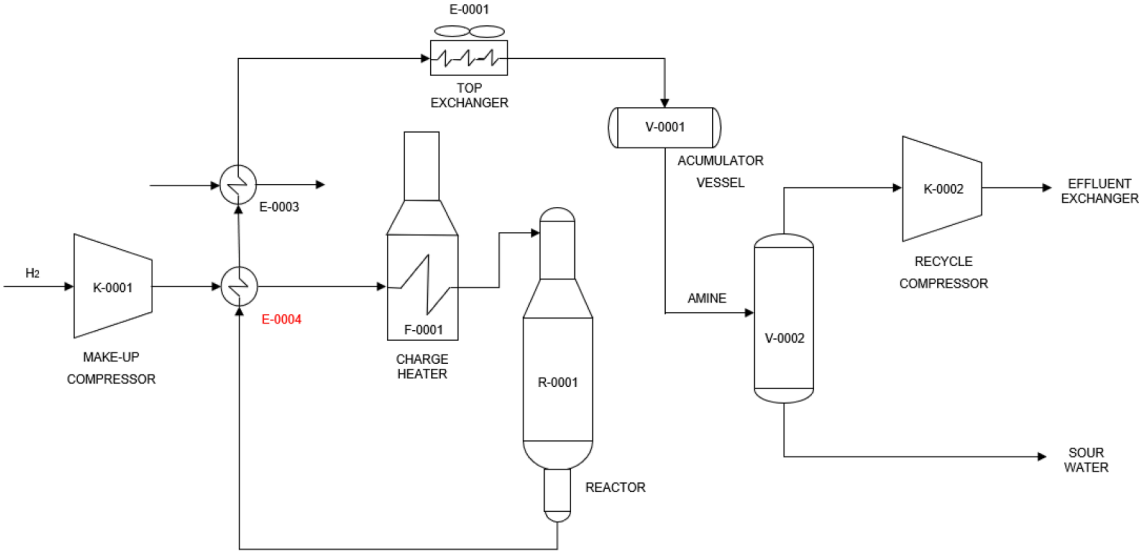

Fig. 1. Schematic flowchart of the diesel hydrotreating unit.

allowing them to separate and disperse in the aqueous solution. Therefore, the water acts as a solvent, separating the ions from the solid salt and allowing them to be present as ions in the solution. This ionic dissociation is a common characteristic of ionic compounds when they are solubilized in water [46].

$$NH_4Cl_{(s)} + H_2O \rightarrow NH^+_{4(aq)} + Cl^-_{(aq)} \quad (2)$$

Chloride ions (Cl^-) can cause corrosion in stainless steels through a process called "pitting corrosion". This occurs when chloride ions accumulate in specific places on the surface of the stainless steel, where conditions favor the formation of small corroded areas called "pits". These pits can grow and deepen, compromising the integrity of the material over time.

Ammonium chloride salts have a whitish, greenish, or brownish appearance. Washing with water or steam will remove the deposits so that during visual inspection it is not evident that the salt deposition process has occurred [47]. Salt corrosion is typically localized and results in pitting corrosion. Corrosion rates can be extremely high [48].

Fig. 2 shows the schematic design of the corrosive process of ammonium chloride in the hydrotreatment section of a diesel production plant [49].

In the refining industry today, corrosion by ammonium chloride is one of the main causes of equipment failures, mainly in heat exchangers, requiring the completion of the tube bundle retubing process [50]. Due to the associated material, maintenance, and repair costs, NH_4Cl corrosion has a devastating impact on petroleum refining plants, it can also cause damage to the structural integrity and compromise equipment safety [51].

In general, the morphology of corrosion caused by NH_4Cl is characterized as localized, which often results in holes or perforations of equipment, leading to a consequent loss of containment [52]. Ammonium salt granules can easily settle on the tube walls and absorb water vapor, thus forming a highly concentrated electrolyte solution, resulting in corrosion failures, causing holes in the tube bundle of oil refinery heat exchangers [53].

The presence of ammonia, hydrogen sulfides, and chlorides in the reaction effluent sections of hydrogenation and petroleum treating units, also called reactor effluent air cooler (REAC) heat exchangers, often causes damage associated with pitting corrosion in various types of equipment such as heat exchangers, air coolers and piping [54]. Some studies have reported that ammonium chloride hygroscopy is a relevant factor in corrosive processes in oil refineries. Experimental results indicate that around 75 % to 80 % relative humidity, the water vapor present in the hydrotreating process streams gradually condenses and the NH_4Cl dissociates [55].

Good design practice for refining units should provide for symmetrical and hydraulically balanced flow inside and outside the heat exchangers. Continuous or intermittent washing of water may be necessary in the effluent to wash the salt deposition. This is called washing water [56], which must be injected upstream of the places of formation and deposition of ammonium salts in the equipment and pipes. Although washing water may be able to reduce the problems of ammonium salt incrustation and deposition that cause

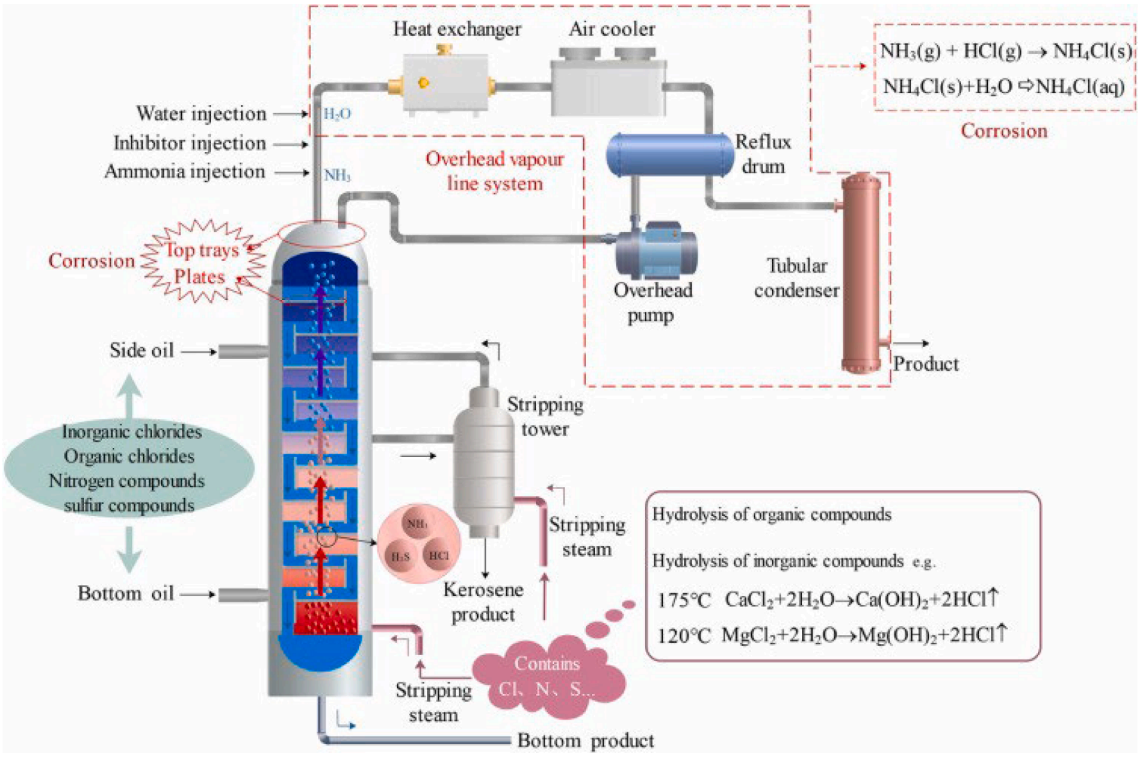

Fig. 2. Schematic design of the corrosion process of ammonium chloride in diesel hydrotreating unit.

corrosion, it can be seen that if this water is used inappropriately and with insufficient flow, it may not solve the problem of ammonium salt deposition and consequent encrustation in equipment [57].

Studies involving failure analysis in oil refining equipment, which process loads with ammonium salt contents, are very common in derivative hydrotreating units, such as diesel and gasoline. Studies indicate that the amount of washing water is sufficient to dissolve ammonium chloride deposits [58]. However, when an atomizing nozzle is not used, the washing water cannot mix effectively with the ammonium chloride, which can lead to equipment failure due to the non-dilution of the ammonium salt particles [59]. Furthermore, the crystallization temperature of ammonium chloride salts increases proportionally with the chloride content in the feed. This is due to higher hydrochloric (HCl) vapor fractions due to chloride content. Thus, NH_4Cl easily crystallizes during the cooling process inside the heat exchanger tubes [60].

Ammonium chloride salt crystallization and deposition occur when the product of the partial pressures of ammonia (NH_3) and hydrogen chloride (HCl) is greater than the stability constant (Kp) of the ammonium chloride salt. The stability constant will depend on the temperature of the medium. Consequently, salt deposition will depend on a set of variables: ammonia and hydrogen chloride concentrations in the vapor state, temperature, and current velocity [61].

2.3. The mechanism of corrosion under deposit

Ammonium chloride corrosion is often in the form of pitting corrosion. Corrosion is one of the most important challenges faced by oil refineries and has received a great deal of attention in recent decades due to the continued dependence of the global economy on petroleum products and natural gas [62]. A review focused on mitigating corrosion in oil refineries is relatively scarce, therefore, gaps in knowledge were identified, especially when addressing ammonium salt corrosion [63].

The hydrogenation reaction is accompanied by the formation of various corrosive gases, in which hydrochloric acid (HCl) reacts with ammonia (NH_3) to form the initial nucleus of ammonium chloride crystals. Due to the intense Brownian motion of the gas in the high temperature environment, the nuclei of NH_4Cl crystals collide and adsorb continuously [64]. Finally, the NH_4Cl particles are condensed into larger particles and become incorporated into the multiphase fluid.

The H^+ ions that occur during electrochemical reactions close to the walls of the materials cause an increase in the mass transfer rate of these ions, which also increases the corrosion rate of the protective film of the metallic wall. The nearby wall is exposed to an acidic aqueous solution that accelerates the corrosion of the metal wall and is characterized by being localized, with consequent perforation of the wall of the heat exchanger tubes of these heat exchangers [65]. However, it is noted that the particles deposited at the bottom of the exchanger tubes are coated by the oil phase of the flow and they cannot effectively absorb the liquid water produced in the environment. Therefore, under-deposit corrosion is likely in the region of the top and sides of the heat exchanger tubes [66].

The ammonium chloride corrosion process in this environment can be divided into phases: In the first phase, it occurs in the reaction section between NH_3 and HCl in the gas phase to form the nucleus of NH_4Cl crystals [67]. Having continuous contact due to flow phenomena and the collision between the nuclei, these formed crystals are bonded to each other and gradually condense to form larger nuclei of NH_4Cl. NH_4Cl absorbs a small amount of free water present in the heat exchanger tube, which does not promote the adsorption of these particles on the upper wall of the tube bundle of these exchangers, but wets the surface of the particles and accelerates their adherence [68].

In the second phase, the liquid water content in the tubes increases due to the decrease in temperature, after the reaction section, in which the precipitation process of the vapor phase occurs in the liquid phase [69]. In the third phase, the adsorption of particles on the wall of the equipment can be observed, and there is a formation of a mixture between water and ammonium salt particles. In the fourth, and last, phase, NH_4Cl hydrolysis occurs, forming ions $(NH_4)^+$ and Cl^-, which react with the metallic surface of the heat exchanger heat exchanger tubes, destroying the passive layer, or surface protective film, by releasing ammonia which accelerates the formation of more ammonium chloride salts [70].

Solid particles of ammonium salt (NH_4Cl) can go through a process of deliquescence before dissolving completely. Deliquescence is a phenomenon in which a hygroscopic solid substance (which has an affinity for water) absorbs moisture from the environment and eventually dissolves in the absorbed water [71]. This process occurs when the relative humidity is high enough for the substance to absorb water from the surrounding air. In conditions of high relative humidity, the solid particles of ammonium chloride absorb moisture from the air, and this causes the particles to start turning into an aqueous solution. As the absorption of water continues, the ammonium chloride dissolves completely in the absorbed water [72].

During deliquescence, the ammonium chloride particles are in direct contact with the water they are absorbing from the environment, and it is at this point that corrosion is most likely to occur. The water acts as a medium that enables the electrochemical reaction that leads to corrosion. To prevent corrosion in environments where ammonium chloride deliquescence is a problem, it is important to take appropriate measures, such as controlling humidity, protecting metals, and using protective coatings if necessary [73].

Deposit corrosion occurs when corrosive materials or solid particles accumulate or adhere to the surface of a metal or material, creating a protective layer that retains moisture or corrosive substances. Deposit corrosion is often observed in industrial environments, where metal surfaces are subject to contamination by waste or chemicals. These deposits accelerate the corrosion process because they isolate the metal surface from the action of oxygen and moisture, creating favorable conditions for localized corrosion [74].

Solution corrosion occurs when a metal reacts directly with substances dissolved in a liquid, such as water. This chemical reaction with the ions presents in the solution causes the metal to deteriorate over time. Water is a common solvent in solution corrosion processes, and the presence of dissolved ions, such as chlorine ions, oxygen ions and others, can accelerate the corrosion process.

Solution corrosion is often observed in submerged metal structures such as bridges, pipelines and industrial equipment that come into contact with water or corrosive liquids [75].

3. Materials and methods

3.1. Materials

AISI 304, AISI 316L and AISI 317L stainless steel samples were obtained from annealed flat metal sheets measuring 500 mm × 500 mm × 6.35 mm. The chemical composition was determined by optical emission spectrometry Spectrotest TXC-03 Spectro Analytical Instruments GmbH.

For corrosion tests and metallography of stainless steels, the samples were cut in dimensions of 10 mm × 10 mm. Then, the samples were cleaned in an ultrasonic bath Ultracleaner, Unique 700. The inputs used were distilled water and liquid detergent, cleaning time of 10 min, and at a temperature of 25 °C. The samples were then submitted to a passivation treatment with 50 % nitric acid at a temperature of 40 °C for 30 min [76].

3.2. Chemical analysis

Residue (corrosion products) and material samples from the load heat exchanger of the diesel hydrotreating unit were collected in locations close to the faulted regions for investigation. Chemical analysis of the anomalous tubes was performed by X-ray fluorescence spectroscopy, Niton Analyzers, Thermo Scientific model XL3t-800. The measurement of thickness in the heat exchanger shell was performed by ultrasound, Krautkramer, model DM4, a head with a diameter of 5 mm with a piezoelectric sensor, and the methylcellulose couplant was used [77]. To determine the integrity of the tube bundle, an eddy current test was performed using the Eddyfi Reddy Ectane equipment. The chemical analysis of the residues found in the heat exchanger was carried out by X-ray fluorescence spectroscopy, Thermo Scientific Flash 2000, also determining the carbon, hydrogen, nitrogen, and oxygen contents.

3.3. Mechanical analysis

The surface hardness measurement of steels is carried out to determine the resistance to penetration of an indenter or penetrator into the surface of a material. During the application of the load, the penetrator penetrates the surface of the material. The depth of penetration is measured by the indentation left by the penetrator on the surface [78]. The hardness is calculated based on the dimensions of the indentation left by the penetrator on the surface of the steel. The Vickers hardness scale, the hardness is calculated from the diagonal of the indentation left by the Vickers penetrator. The hardness of the samples was determined using a Vickers microhardness tester, Shimadzu, HMV-2TE, with a 40x magnification lens, diamond-tipped indenter, 15 s penetration time and an applied load of 2,942 N, in which 10 measurements were taken on the surface of the samples.

Metallographic analysis of stainless steels involves the preparation of steel samples, followed by microscopic observation to evaluate the microstructure, composition, and characteristics of the material. The following steps were taken during sample preparation: cutting, where samples were cut in the dimension 10 mm × 10 mm × 6.54 mm using a mechanical cutter and a diamond abrasive cutting disc, the cold embedding stage involved the application of a self-curing chemically active acrylic type resin, brand JET, model X15, accompanied by the addition of a polymerizing methyl methacrylate catalyst [79].

The sanding stage of the sample surface is achieved by using progressive sandpaper with abrasives of increasing granulometry to remove any cut marks and obtain a flat, polished surface. The polishing process was carried out using increasingly fine abrasives to obtain a mirror-like surface, which will enable the formation of an image suitable for micrography tests. The samples were then subjected to the conventional metallographic preparation of grinding and polishing with 9 μm, 3 μm and 1 μm diamond paste and etching [80]. To reveal the microstructure, the sample is subjected to a chemical attack.

The type of chemical attack to be used depends on the specific stainless steel and the objectives of the analysis. The chemical attack can be acidic, alkaline, or electrolytic and helps to reveal the grain contours and other features of the microstructure. In this research, the use of nitric acid and hydrochloric acid was adopted. The etching solution was prepared minutes before carrying out the etching process and revealing the samples. The microstructures were observed using optical microscopy, Kontrol, model LM-719, digital camera MDCE-5A.

3.4. Electrochemical methods

Electrochemical corrosion tests are a class of experimental methods used to study and evaluate the corrosion of metallic materials. These tests involve measuring electrical currents and potentials associated with corrosion in electrochemical systems [81]. They are often used to determine the corrosion rate, corrosion resistance and electrochemical behavior of materials under different conditions. In this work, electrochemical polarization techniques were applied, which is a common test that involves applying a controlled variation in electrical potential to a metal sample immersed in a corrosive electrolyte [81]. The electrochemical response of the sample, measured in terms of electric current, is recorded. This makes it possible to determine the anodic and cathodic polarization, as well as the corrosion rate of the material at different potentials. The electrochemical impedance technique was also applied, which are tests that involve applying a small alternating potential variation to the sample and measuring the resulting electrical impedance. Electrochemical impedance analysis provides information on corrosion resistance, reaction kinetics and the capacitance of the metal-

electrolyte interface [82].

Electrochemical corrosion tests were conducted by potentiodynamic polarization and electrochemical impedance spectroscopy, Vertex potentiostat/galvanostat, IVIUM Technologies, with electrochemical cell, 250 mL, with 3 electrodes: Ag/AgCl reference electrode (RE), XH286, RE-1B; against a spiral platinum electrode (CE) with 65 mm in length and 0.5 mm in thickness and the working electrode (WE) were the samples of the analyzed stainless steels. The chemical solutions used were obtained with sodium chloride analytical reagent, Exodus Científica, ammonium chloride (NH_4Cl), Vetec Química and distilled water. The parameters used in the potentiodynamic polarization technique were current of 100 mA, potential sweep scan rate of 0.16 mV/s. Before experiments, the open circuit potential (OCP) was monitored at least 60 mins until a steady state was reached and potential variation range from −0.5 V (vs OCP) to +0.7 V (vs OCP) [83]. The parameters used in the electrochemical impedance spectroscopy (EIS) technique were open circuit potential as a reference, frequency range between 1,000,000 Hz (1 MHz) and 0.01 Hz (10 mHZ), 10 steps per decade of frequency and potential amplitude of 10 mV (vs OCP), the electrochemical impedance spectroscopy were recorded alternately at different time intervals [84].

The corrosion potential (E_{corr}) and corrosion current density (i_{corr}) were obtained by the intersection of the anode polarization curve with the cathodic polarization curve, namely the Tafel extrapolation technique [85]. Other parameters, such as the pit potential (E_{pit}) and the Tafel constants were obtained graphically. After testing, the morphologies of the corrosion generated were analyzed by scanning electron microscopy, SEM EVO MA 10 Carl Zeiss.

The Stern-Geary equation, also known as the simplified Tafel equation, is an empirical relationship used in electrochemistry and corrosion to calculate the corrosion rate of a metal based on electrochemical parameters [86]. The equation is a simplified form of the Tafel equation and is often used when there is limited data on the electrochemical behavior of the system. This equation is used to estimate the corrosion rate from measurements of the metal's corrosion potential and the Stern-Geary constant, which is determined experimentally. According to the Stern-Geary formula as shown in Equation (3), the relationship between the corrosion current density Icorr of the corroded metal electrode and the polarization resistance Rp is as follows [87]:

$$i_{corr} = \frac{\beta a.\beta c}{2.303.(\beta a + \beta c)} \bullet \frac{1}{R_p} \tag{3}$$

where i_{corr} is the corrosion current density in (A cm^{-2}).

β_a is the slope of the anodic polarization curve (V/dec) - can be obtained experimentally.

β_c is the slope of the cathodic polarization curve (V/dec) - also obtained experimentally.

R_p is the polarization resistance (ohms).

A corrosion equivalent circuit is a simplified representation of the electrochemical properties of a corrosion system, which is often used to model and understand corrosion behavior. When analyzing a corrosion equivalent circuit, the following parameters are commonly obtained, such as: polarization resistance (R_p), this parameter represents the resistance to the passage of electric current that is applied to a corrosion system [88]. It reflects the difficulty that electrons face when passing through the corroded metal surface and corrosion products. Solution resistance (Rs), this resistance is associated with the ionic conductivity of the electrolyte (usually an aqueous solution) surrounding the corrosion system. The solution resistance influences the ability of ions to move in the electrolyte and thus affects the corrosion rate [89]. The double layer capacitance (CPE) is a parameter that reflects the capacity of the metal-solution interface to store electrical charges. It is related to the formation and structure of the electrical double layer. Capacitance is measured in farads (F) and can influence the behavior of the corrosion reaction [90].

The corrosion potential (E_{corr}) is the electrochemical potential at which the corrosion rate is minimal, and the corrosion reaction and the surface protection reaction (such as the formation of the passive layer) are in equilibrium. It is a critical parameter that indicates the corrosion tendency of the system [91]. The corrosion current (i_{corr}) is the rate at which electrons flow in the corrosion system due to the electrochemical corrosion reaction. It is a direct indicator of the corrosion rate. Open circuit potential (OCP) is the electrochemical potential of the system when it is not subject to external polarization. It is measured when no current is flowing and can provide information on the corrosion state of the system [92]. And current density is the current per unit area flowing on the surface of the corroded material. It is related to the corrosion rate and is expressed in (A. cm^{-2}). These parameters are essential for analyzing and modeling the corrosion behavior of metallic materials. A corrosion equivalent circuit can be used to estimate these parameters based on experimental data and is valuable for understanding how conditions and properties affect the corrosion rate and corrosion protection [93].

4. Results

4.1. Chemical composition of the residue

The results of the chemical analysis are shown in Table 1.

Table 1
Chemical analysis of the heat exchanger residue E-0004.

Compounds/Element	Cr_2O_3	Fe_2O_3	$FeCl_2$	Carbon	Nitrogen	Sulfur
Content (wt%)	15.6	16.7	24.7	29.4	12.9	0.32

The results of the X-Ray Fluorescence Spectrometry test performed on the heat exchanger residue (corrosion products) sample indicated the presence of the following chemical elements, carbon, hydrogen, nitrogen, and sulfur. The residue found had the characteristics of a finely dispersed powder. The carbon and sulfur found during the chemical analysis are possible contaminants of the diesel stream in the residue sample obtained. It is known that diesel can contain sulfur as a result of the petroleum refining process. The sulfur content in diesel varies depending on the regulatory specifications of each refining country [94].

The nature and specific composition of the corrosion products in ammonium chloride corrosion can vary depending on conditions such as temperature, ammonium chloride concentration, pH and the metal material involved [95]. In addition, the formation of corrosion products can be complex and depend on factors such as the presence of impurities or alloying elements in the metal. Metallic chlorides of the $FeCl_2$ type (ferrous chloride) can be seen in corrosion products. Ammonium chloride is a source of chloride ions that can react with the metal to form metal chlorides [96]. The formation of metal chlorides, such as iron chloride ($FeCl_2$ or $FeCl_3$) in steel, is common during ammonium chloride corrosion. The corrosion product detected was in the form of crystalline solids, such as white adherent solids. Austenitic stainless steels have the ability to form a passive oxide layer on the surface, usually chromium oxide (Cr_2O_3), this formation may be a reaction to exposure to different corrosive media [97].

4.2. Chemical composition of the tube bundle

The results of the chemical composition of the tube bundle are shown in Table 2.

The chemical composition of the E-0004 heat exchanger tubes is within the specifications of the standard for heat exchanger tubes in austenitic stainless steel according to ASTM classification A-213 Tp 304 [98]. ASTM A213-304 steel is an austenitic stainless-steel alloy that is commonly used in applications requiring corrosion resistance and high durability in challenging environments. It is important to note that the exact specifications for ASTM A213 Tp 304 steel may vary slightly depending on the manufacturer and the specific application.

This respective standard covers a wide range of alloy steel tubes, including ferritic, austenitic and carbon steel stainless steels. It specifies detailed requirements for dimensions, mechanical properties, chemical composition, testing methods and dimensional tolerances of tubes.

4.3. Eddy current testing in the tube beam

The result of the eddy current test performed on the tube bundle can be seen in Table 3.

The eddy current test is performed on heat exchanger tubes to assess the structural integrity and detect possible defects in the tubes [99]. Based on the results of the test carried out, it can be inferred that about 73 tubes have loss of wall thickness of up to 20 %, that is, 0.42 mm, which is 34.4 % of the total number of tubes. Approximately 44 tubes have wall thickness loss of up to 40 %, that is, 0.84 mm, which is 20.8 % of the total number of tubes. Almost 37 tubes have wall thickness loss of up to 60 %, that is, 1.27 mm, which is 17.5 % of the total number of tubes. Approximately 23 tubes have wall thickness loss of up to 80 %, that is 1.68 mm, which is 10.8 % of the total number of tubes. Around 14 tubes have wall thickness loss of up to 100 %, that is, 2.11 mm, which is 6.6 % of the total number of tubes. Moreover, approximately 21 tubes showed an obstruction process, which prevented the possibility of carrying out the eddy current test in these respective tubes, which corresponded to 9.9 % of the total number of tubes in the heat exchanger tube bundle.

4.4. Ultrasonic shell thickness measurement

The sites where the thickness was measured by ultrasound along the shell of the E-0004 heat exchanger are shown in Fig. 3.

Ultrasonic thickness measurement testing is a non-destructive inspection (NDT) technique widely used on equipment, structures, and components to determine the thickness of materials, usually metals, but it can also be applied to other materials. The main purpose of this test is to assess structural integrity, identify wear, corrosion or erosion, and monitor thickness over time. The points numbered 1 to 6 indicate the locations at which the test was actually carried out; these are the equipment's thickness measurement control points [100]. The ultrasound thickness measurement testing plays a key role in preventive maintenance and ensuring the integrity of equipment and structures, helping to avoid accidents and extend the useful life of industrial assets. In the Fig. 2 shows the components known as the hull and head.

The result of the ultrasound thickness measurement test on the heat exchanger shell can be seen in Table 4.

It should be mentioned that the upper region of the equipment shell (points identified by 2 and 4) was more affected by the loss of thickness process, especially close to the shell flange. The point 2 was below the minimum thickness but point 4 is still within the acceptable limit. Ultrasonic thickness measurement is a non-destructive testing technique that measures the thickness of a material, with access to only one side of the part or equipment to be measured [101]. It can be observed that one of the corrosive effects in thermal exchange equipment subjected to fluxes containing ammonium chloride is localized corrosion and the subsequent occurrence

Table 2
Chemical composition of the heat exchanger tubes E-0004 (wt. %).

Element	C	Mn	Ni	Si	P	S	Cr
Content (wt%)	0.07	1.47	8.05	0.52	0.021	0.008	18.4

Table 3
Result of the eddy current test on the tube beam.

Loss of thickness in tubes (%)	Quantity of tubes
0–20	73
21–40	44
41–60	37
61–80	23
81–100	14
Obstruction tubes	21
Total number of tubes	212

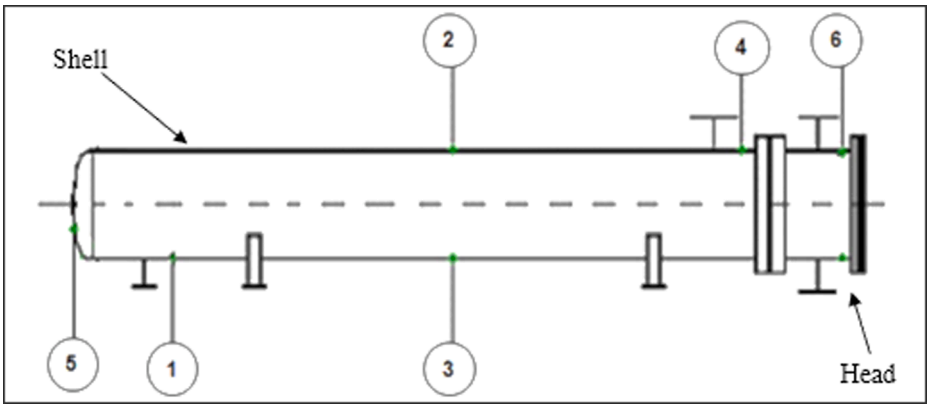

Fig. 3. Indication of the places where the ultrasonic test was performed on the heat exchanger shell E-0004.

Table 4
Result of thickness measurement test on the heat exchanger shell.

Measurements	1	2	3	4	5	6
Nominal thickness (mm)	44.00	12.50	12.50	12.50	12.50	9.50
Minimum design thickness (mm)	41.00	9.50	6.50	6.50	6.50	3.50
Measurement value (mm)	50.10	8.20	9.30	7.30	9.60	11.30

of loss of metallic material from the steel surface, which is why areas inside the shell with regions with loss of thickness were identified [102]. As a temporary measure, at the most critical points of loss of thickness, structural reinforcement plates were installed to increase the thickness and plan for the development of studies to modify the material previously used in this equipment.

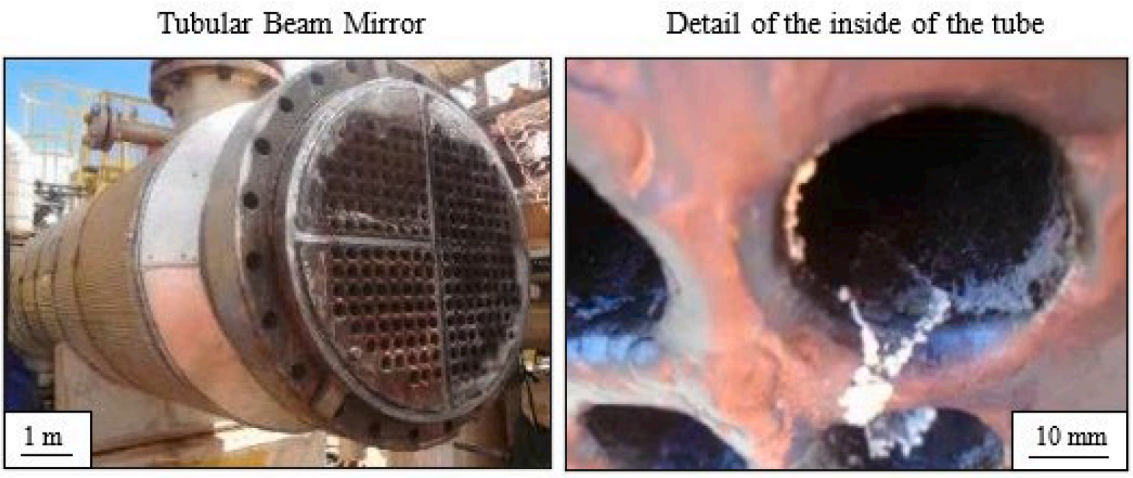

Fig. 4. Presence of adherent residue on the surface of the tube beam mirror of the load preheater heat exchanger (E-0004).

4.5. Internal and external visual inspection of the tube beam and shell

Fig. 4 shows an overview after disassembling the spool and exposing the tubular beam mirror.

The presence of adherent residue on the surface and inside the shell of the load pre-heater heat exchanger (E-0004) was observed, appearing as a fine white powder, associated with ammonium chloride [103]. Internally, a large amount of white salt deposits was observed in the tubes, concentrated in the lower part (product outlet). This product was wet and well- compacted.

Fig. 5 shows an internal and external view of the load preheater heat exchanger shell (E-0004). On the left, the inner region of the shell after removing the tube beam for the retubing and internal washing process, images (a) and (c). On the right, the region of failure and installation of the protection plate, in places of intense corrosion, images (b) and (d).

Pitting corrosion can be observed. It is a form of localized corrosion that can occur in the shell of heat exchangers [104]. This form of corrosion is characterized by the formation of small cavities or pits on the metallic surface, resulting from the selective corrosion of certain materials, as seen in Fig. 4(c), (d). Pits formed by pitting corrosion tend to be small, irregularly shaped, and may spread across the metal surface. These pits can sink deep into the thickness of the metal, compromising its structural integrity. In some cases, the pits can join together, forming corrosion channels [105].

Fig. 6 shows the tube bundle of this heat exchanger. It was observed that the tubes were totally impregnated with salts and with an intense corrosion process.

The exchanger tube bundles had to be completely changed due to the fact that the remaining life was less than an operational campaign. The tubes showed a loss of thickness below that recommended by the TEMA (Tubular Exchanger Manufacturers Association) construction standards [106] for shell and tube heat exchangers, including perforated tubes, as demonstrated in the eddy current test (Table 3).

4.6. Chemical composition of austenitic stainless-steel samples

The chemical compositions of the tested stainless-steel samples are shown in Table 5.

The values obtained were compared with the values indicated by the ASTM A213 standard, which establishes the chemical requirements for the composition of different types of stainless steel, including the limits of chemical elements such as carbon,

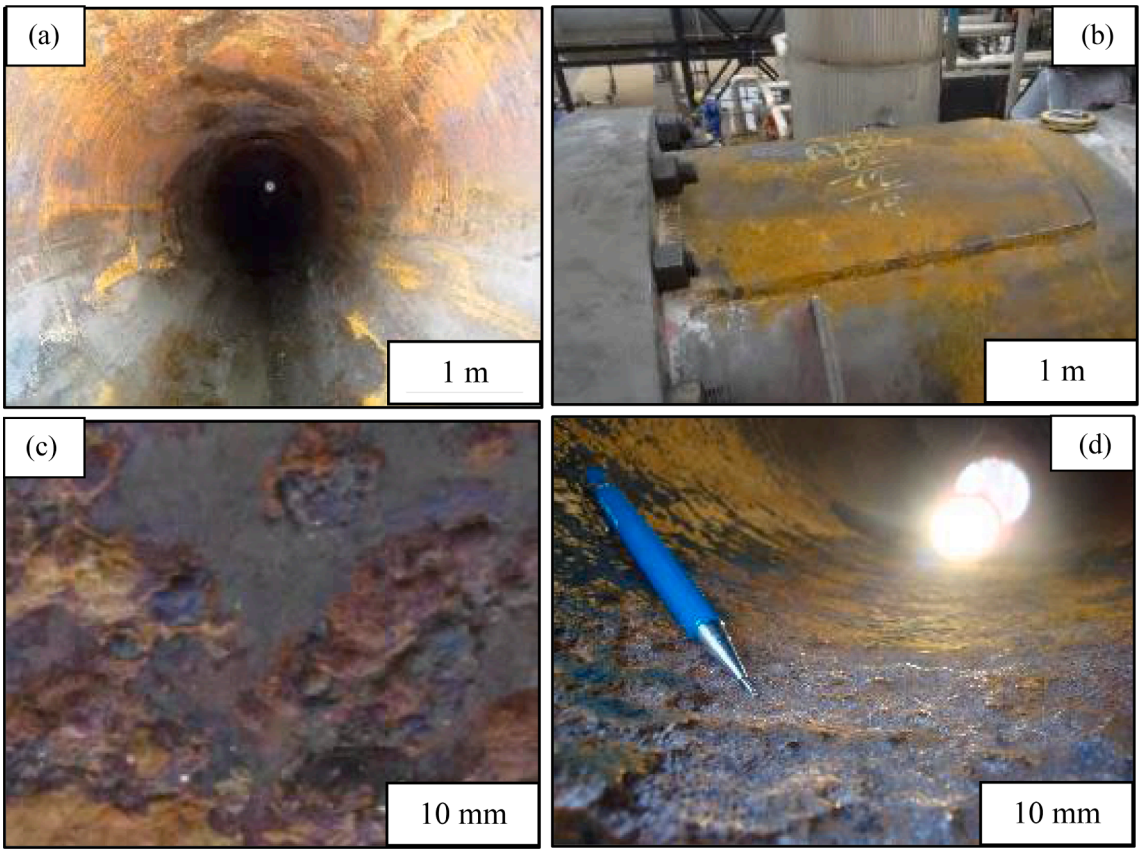

Fig. 5. Internal and external view of the load preheater heat exchanger shell (E-0004) and failure region: a) general internal view, b) external view after repair, c) and d) internal view at different magnifications.

Fig. 6. External visual analysis of the load heat exchanger tube bundle (E-0004).

manganese, phosphorus, sulfur, silicon, chromium, nickel, molybdenum, and other chemical elements. It can be observed that the chemical composition of the steel samples is within the ranges allowed by the standard for heat exchange tubes for high temperature and corrosive services [107], with Tp 304, 316L, 317L classification.

4.7. Metallographic and microhardness analysis of austenitic stainless-steel samples

Fig. 7 shows the microstructures obtained from the samples for the three analyzed steels, 304, 316L and 317L.

The revealed morphologies show that they are typical microstructures of austenitic stainless steels [108]. These crystalline structures observed have a fine and homogeneous granular microstructure, the grains have well-defined and rounded edges, which are the result of the controlled heating and cooling process during the manufacturing process [109].

Austenitic stainless steels, such as 304, 316L and 317L, have a typical crystalline microstructure composed mainly of austenite crystals. Austenite is a form of face-centered cubic (CFC) crystal and is known for its stability at high temperatures and its ability to resist corrosion. The crystalline microstructure of these stainless steels is one of the reasons why they are widely used in applications that require corrosion resistance.

The results of the Vickers microhardness measurement are shown in Table 6.

Table 5
Chemical composition of the samples (wt. %).

Element	Fe	C	Cr	Ni	Mn	Co	Mo
304	71.10 ± 0.32	0.027 ± 0.001	18.43 ± 0.18	7.98 ± 0.21	1.54 ± 0.15	0.24 ± 0.17	0.08 ± 0.03
316L	69.21 ± 0.26	0.034 ± 0.002	16.57 ± 0.16	9.79 ± 0.18	1.31 ± 0.12	0.23 ± 0.14	2.05 ± 0.02
317L	63.7 ± 0.24	0.036 ± 0.001	18.49 ± 0.15	11.69 ± 0.19	1.94 ± 0.12	0.08 ± 0.16	3.16 ± 0.03

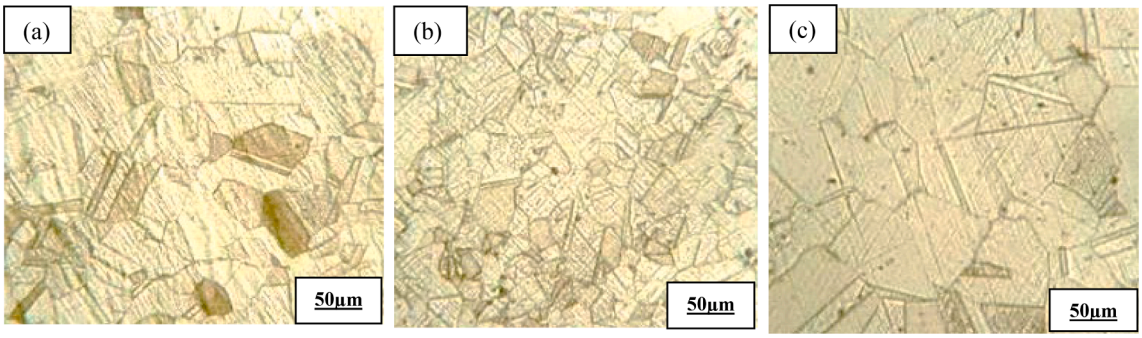

Fig. 7. Microstructures obtained for austenitic stainless steels 304 (a), 316L (b) and 317L (c).

The relationship between hardness and corrosion capacity is multifaceted and depends on several factors, including composition, microstructure, exposure environment and the specific type of corrosion. In many cases, hardness can contribute to corrosion resistance, but it is not the only determining factor. For stainless steels, the formation of a protective oxide layer (passivation) on the surface is fundamental to resisting corrosion. Materials with greater hardness can be more resistant to the penetration of ions or corrosive particles, which can protect the passive layer and therefore increase corrosion resistance [110].

Austenitic stainless steel 304 has a lower average hardness value, which makes it relatively soft compared to other stainless steels. This low hardness can be attributed to its chemical composition, which contains low levels of molybdenum and nitrogen, and to the fact that this steel is not hardened by heat treatment. On the other hand, the 316L and 317L austenitic stainless steels have higher hardness values than the 304 steel, which is partly due to the presence of higher molybdenum and nitrogen contents in their chemical composition, which contribute to corrosion resistance, increased hardness and provide greater mechanical resistance. In summary, both 316L and 317L stainless steels have similar Vickers microhardness, ranging from 150 HV to 220 HV [111]. Both steels have good corrosion resistance, in which 317L steel is particularly suitable for aggressive chemical environments and high temperatures due to its higher molybdenum content. It is important to point out that the Vickers microhardness values may vary depending on the specific manufacturing process, heat treatment and chemical composition of each batch of steel.

4.8. Electrochemical corrosion tests

4.8.1. Potentiodynamic polarization tests

Fig. 8 shows the potentiodynamic polarization curves of samples of material 304, 316L and 317L exposed to an aqueous medium of sodium chloride and ammonium chloride.

The results of the corrosion tests using the potentiodynamic polarization technique carried out on metallic samples of different types of materials are summarized and shown in Table 7. It should be mentioned that the average values between the three samples tested for each experimental condition are available. The corrosion rate (CR), millimeters per year (mm.year^{-1}), refers to the amount of material corroded in millimeters each year.

The corrosive behavior of metallic samples in austenitic stainless steel 304 showed similar results for both aqueous exposure media, sodium chloride and ammonium chloride. The presence of small variations in the corrosion potential parameters from −0.260 V to −0.195 V was observed. The current density variation obtained was from 1.906×10^{-7} A cm^{-2} to 6.972×10^{-8} A cm^{-2}. The variation in the corrosion rate (CR) was from 2.524×10^{-3} mm year^{-1} to 8.442×10^{-4} mm.year^{-1} and the variation in the pitting potential obtained was from +0.150 V to +0.300 V. Thus, the stainless material presented similar behavior in the two electrochemical electrolytes.

The corrosive behavior of metallic samples in austenitic 316L stainless steel showed similar results for both aqueous exposure

Table 6
Results of the Vickers microhardness measurement of the samples.

Measurement	304	316L	317L
1	161	177	190
2	186	180	181
3	171	175	171
4	186	182	186
5	174	182	192
6	166	192	192
7	165	185	189
8	172	181	192
9	169	176	190
10	167	194	184
Average	172 ± 8	182 ± 6	187 ± 6

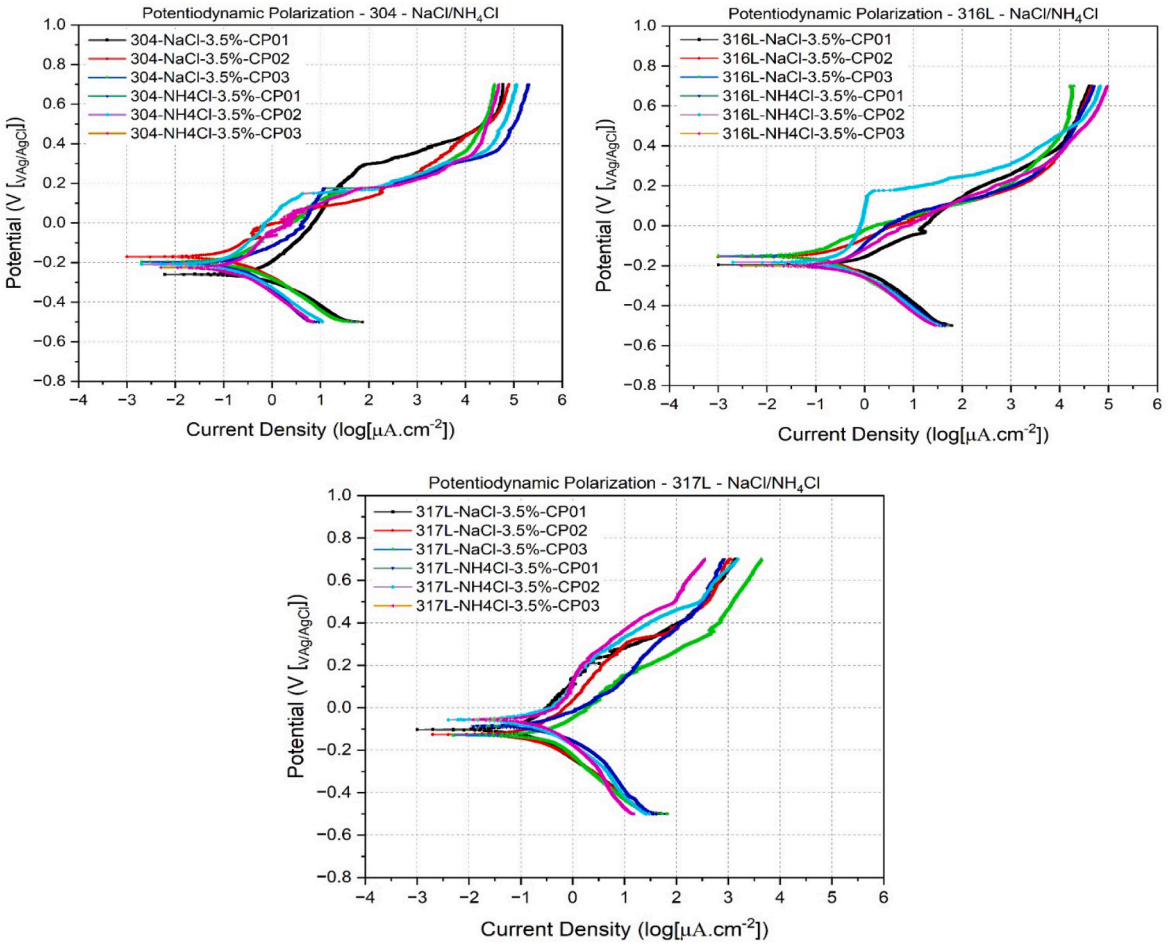

Fig. 8. Polarization curves of the 304, 316L and 317L stainless steel samples in NaCl and NH_4Cl.

Table 7
Results of the potentiodynamic polarization corrosion tests.

Samples	Corrosion Potential [E_{corr}] (V)	Current Density [i_{corr}] log(μA.cm^{-2})	Corrosion Rate [CR] (mm.year^{-1})	Pitting Potential [E_{pit}] (V)	Anode Slope [β_a] (V/dec)	Cathode Slope [β_c] (V/dec)
304-NaCl	−0.260	6.754×10^{-8}	8.442×10^{-4}	+0.195	0.051	0.055
304-NH_4Cl	−0.205	4.227×10^{-7}	7.910×10^{-3}	+0.170	0.071	0.059
316L-NaCl	−0.175	2.681×10^{-8}	4.810×10^{-4}	+0.115	0.081	0.067
316L-NH_4Cl	−0.205	2.309×10^{-7}	2.682×10^{-3}	+0.110	0.076	0.071
317L-NaCl	−0.120	2.825×10^{-8}	1.281×10^{-4}	+0.430	0.078	0.073
317L-NH_4Cl	−0.085	4.426×10^{-8}	1.163×10^{-4}	+0.470	0.076	0.069

media. The presence of small variations in the corrosion potential parameters from 0.205 V to −0.170 V was observed. The current density variation obtained was from 1.194×10^{-7} A cm^{-2} to 4.141×10^{-8} A cm^{-2}. The corrosion rate (CR) variation was from 1.387×10^{-3} mm/year to 4.810×10^{-4} mm.year^{-1} and the pitting potential variation obtained was from +0.085 V to +0.180 V.

The corrosive behavior of metallic samples in austenitic 317L stainless steel showed similar results for both aqueous exposure media. The presence of small variations in the corrosion potential parameters from −0.120 V to −0.085 V. The current density variation obtained was from 2.243×10^{-8} A cm^{-2} to 6.845×10^{-8} A cm^{-2}. The corrosion rate (CR) variation was from 2.606×10^{-4} mm.year^{-1} to 7.950×10^{-4} mm.year^{-1} and the pitting potential variation obtained was from +0250 V to +0500 V.

The addition of molybdenum, as in 317L steel, increases the material's resistance to non-oxidizing acidic atmospheres, localized corrosion, and resistance to high temperatures. The polarization resistance in a potentiodynamic polarization corrosion test was calculated from the relationship between the applied potential difference and the polarization current flowing through the sample [112]. This resistance can be used to determine the corrosion rate and the kinetics of electrochemical reactions on metallic surfaces

[113].

The Tafel curves, which consist of two straight lines, the anode straight line and the cathodic straight line, correspond to the electrochemical reactions occurring at the anode and cathode, respectively. The anode slope and the cathode slope in the Tafel curves are important parameters that describe the electrochemical corrosion reaction rate in each of the regions [114]. The anode slope is the one of the Tafel curve in the anode region, which represents the oxidation rate of the material. This slope is proportional to the speed of the anode reaction and is expressed in terms of a constant of proportionality called the electron transfer factor [115]. In turn, the cathode slope is the one of the Tafel curve in the cathode region, which represents the reduction rate of the material. This slope is proportional to the speed of the cathodic reaction and is expressed in terms of a constant of proportionality called the mass transfer factor. Note that the values of these slopes are consistent with those indicated in the literature for corrosion tests using austenitic stainless steels [116].

It can be observed that the values obtained for the 317L austenitic stainless steel showed greater corrosion resistance capacity than the 304 and 316L stainless steels, exposed to a medium containing sodium chloride and ammonium chloride, which was corroborated by the high values obtained for the pitting potential of this steel in question and the corrosion rate; the lower the corrosion rate, the greater the corrosion resistance [117].

Regarding the thermodynamic parameter of corrosion potential (E_{corr}), for the medium containing sodium chloride, the samples of austenitic stainless steel 304 showed average values of -0.23 ± 0.02 V, while the samples of 316L stainless steel showed an average value of -0.19 ± 0.04 V for the corrosion potential and finally, the 317L stainless steel samples showed an average value of -0.11 ± 0.03 V for the corrosion potential.

Samples with higher corrosion potential values indicate a lower tendency for these materials to corrode and are more resistant to corrosive attacks [118]. In the electrochemical medium of sodium chloride, the corrosion density values (i_{corr}) for the austenitic 304 and 316L stainless steels presented values with an order of magnitude ranging between 10^{-7} and 10^{-8}. On the other hand, the 317L material showed values in the order of magnitude predominantly of 10^{-8}. In relation to the ammonium chloride electrolyte, the corrosion density values for the austenitic 304 stainless steels (only one sample) presented values with an order of magnitude in 10^{-7} and the other samples presented an order of 10^{-8}.

For the austenitic 304 and 316L stainless steel samples, the corrosion rates (mm/year) obtained vary in the order of magnitude between 10^{-3} and 10^{-4}. The 317L stainless steel sample showed predominantly the lowest corrosion rates of the tested samples that were in the order of magnitude 10^{-4}. The pitting potential (E_{pit}) of the austenitic 304 stainless steel samples showed an average value of -0.18 ± 0.03 V, while the 316L stainless steel samples showed an average value of -0.11 ± 0.02 V for the corrosion potential and finally, the 317L stainless steel samples showed an average value of -0.45 ± 0.04 V for the corrosion potential.

The material analyzed among the three austenitic stainless steels, which presents the greatest uniformity, and the analysis parameters of corrosive behavior is the austenitic 317L stainless steel in both exposure media (NaCl and NH_4Cl). This observed result is corroborated by research in the literature, possibly due to the high percentage content of the molybdenum element that has the function of increasing corrosion resistance in an acid medium, particularly the formation of pits in stainless steels [119].

4.8.2. Electrochemical impedance spectroscopy (EIS) tests

For all samples, the RC series–parallel or resistive/capacitive model was adopted [120]. The results of the tests were summarized and shown in Table 8. The average values among the three samples tested for each experimental condition were used.

In an electrochemical corrosion test, the resistance parameter of the electrolytic solution refers to the electrical resistance presented by the solution in which the test is being performed. The solution resistance is a property that affects the load transfer rate during the electrochemical test, the electrolytic solution is responsible for providing the medium in which the electrochemical corrosion reaction takes place [121]. The polarization resistance parameter refers to the additional electrical resistance encountered during the electrochemical polarization process. This resistance is due to several factors, such as ohmic resistance, contact resistance, passive film resistance and electrode/solution interface resistance [122]. Bias resistance affects the electrochemical response of the system during the electrochemical corrosion test. By analyzing the resulting polarization curves, information can be obtained about the corrosion rate, passive film resistance and other relevant parameters. Finally, the capacitance parameter refers to the electrical load storage capacity in an electrochemical system [123]. It is related to the electrical response of the system to potential variations applied during the test. Capacitance is influenced by the nature of the electrochemical system, including the chemical composition of the electrolytic

Table 8
Electrochemical impedance spectroscopy results.

Samples	Electrolyte Solution Resistance [Rs] (Ohm cm^{-2})	Polarization Resistance [Rp] (Ohm cm^{-2})	Capacitance [CPE] (F cm^{-2})
304-NaCl	2.618×10^2 ($\pm$0.03)	7.896×10^3 ($\pm$0.02)	2.130×10^{-4} ($\pm$0.01)
304-NH_4Cl	7.842×10^2 ($\pm$0.02)	9.513×10^4 ($\pm$0.01)	1.126×10^{-4} ($\pm$0.01)
316L-NaCl	1.543×10^2 ($\pm$0.01)	3.087×10^3 ($\pm$0.03)	2.754×10^{-4} ($\pm$0.03)
316L-NH_4Cl	4.810×10^2 ($\pm$0.01)	3.322×10^4 ($\pm$0.01)	2.583×10^{-4} ($\pm$0.02)
317L-NaCl	1.147×10^2 ($\pm$0.02)	1.816×10^5 ($\pm$0.01)	8.639×10^{-4} ($\pm$0.01)
317L-NH_4Cl	7.284×10^2 ($\pm$0.02)	9.815×10^4 ($\pm$0.03)	1.919×10^{-4} ($\pm$0.02)

solution, the properties of the electrode/solution interface and the structure of the material under test [124].

Fig. 9 shows the Nyquist diagrams of the electrochemical impedance spectroscopy tests for the 304, 316L and 317L austenitic stainless-steel samples in aqueous medium of sodium chloride (NaCl) and ammonium chloride (NH_4Cl).

The comparison of the impedance values (real and complex) leads us to infer that for the austenitic stainless steels analyzed, the exposure in an aqueous medium containing sodium chloride solution showed lower values in relation to the exposure of materials to an aqueous medium containing ammonium chloride solution, lower values of the complex impedance parameter (imaginary Z_2 axis), characteristic of the electrochemical kinetic processes [125]. There is also a greater variation in this impedance for the 304 stainless steels followed by the 316L steel, which has a smaller variation in the complex impedance values. However, for the 317L stainless steel, the complex impedance values obtained during the sample test show a relative approximation between the obtained values. This behavior is described by the similarity of the corrosive behavior of this material in both electrochemical means of exposure. Ammonium chloride is a substance that contains chloride ions and ammonium ions. In solution, ammonium ions can form complexes with iron ions on the stainless-steel surface, which can lead to dissolution of the iron and the formation of porosities on the surface [126]. Furthermore, the chloride ions in ammonium chloride can also contribute to the corrosion of stainless steel, as they can act as aggressive agents and destabilize the passive oxide layer that protects the metal from corrosion [127].

Electrical resistance may vary depending on the chemical composition and microstructure of the materials. In general, 317L stainless steel has a higher electrical resistance than 304 and 316L stainless steels. The impedance of stainless steels may vary depending on the chemical composition and microstructure of the materials. In general, test results indicated that 317L stainless steel has a higher impedance than 304 and 316L stainless steels. Thus, it can be inferred that the 317L austenitic stainless steel, under the test conditions proposed in this work, showed greater resistance to corrosion mechanisms for both solution media used (sodium chloride and ammonium chloride) in line with published results [128].

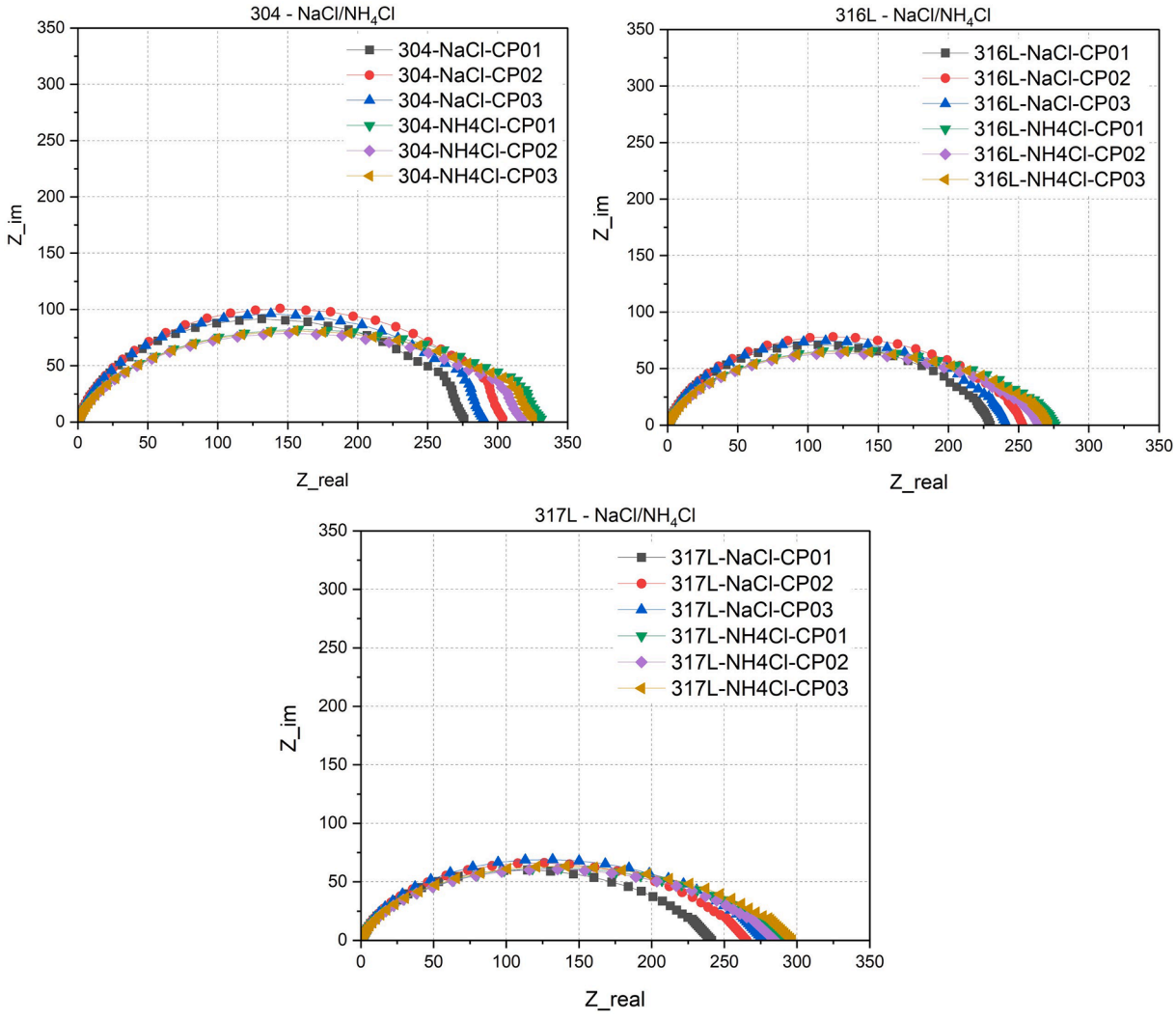

Fig. 9. Nyquist diagrams of the steel samples 304, 316L and 317L in NaCl and NH_4Cl.

In general, the Nyquist diagrams obtained from the analyzed austenitic stainless-steel samples showed a single semicircle, and this is represented by the similarity of the distribution of the points of the curves in the real plane, defined by the impedance variable (Z_1) and in the complex plane, defined by impedance variable (Z_2). Note that all results obtained were corrected by the variable area of exposure to the electrochemical environment (chemical solution or electrolyte) [129,130].

4.9. Analysis of the corrosion surface of the samples with SEM

Fig. 10 shows the images obtained by scanning electron microscopy (SEM) of the 304, 316L and 317L steels, after the polarization test, for NaCl and NH_4Cl media. The images on the left, (a), (c) and (e) represent the exposure in NaCl and the images on the right, (b), (d) and (f), exposure to NH_4Cl. The images (a); (b) are made of 304 steel, images (c); d) 316L steel and images (e); (f) 317L steel.

By analyzing the images obtained from the characterization of the metallic surfaces after the corrosion tests, all finalized in the potentiodynamic polarization at a potential of 0.6 V, it can be observed that the high intensity of the corrosive process in its form by

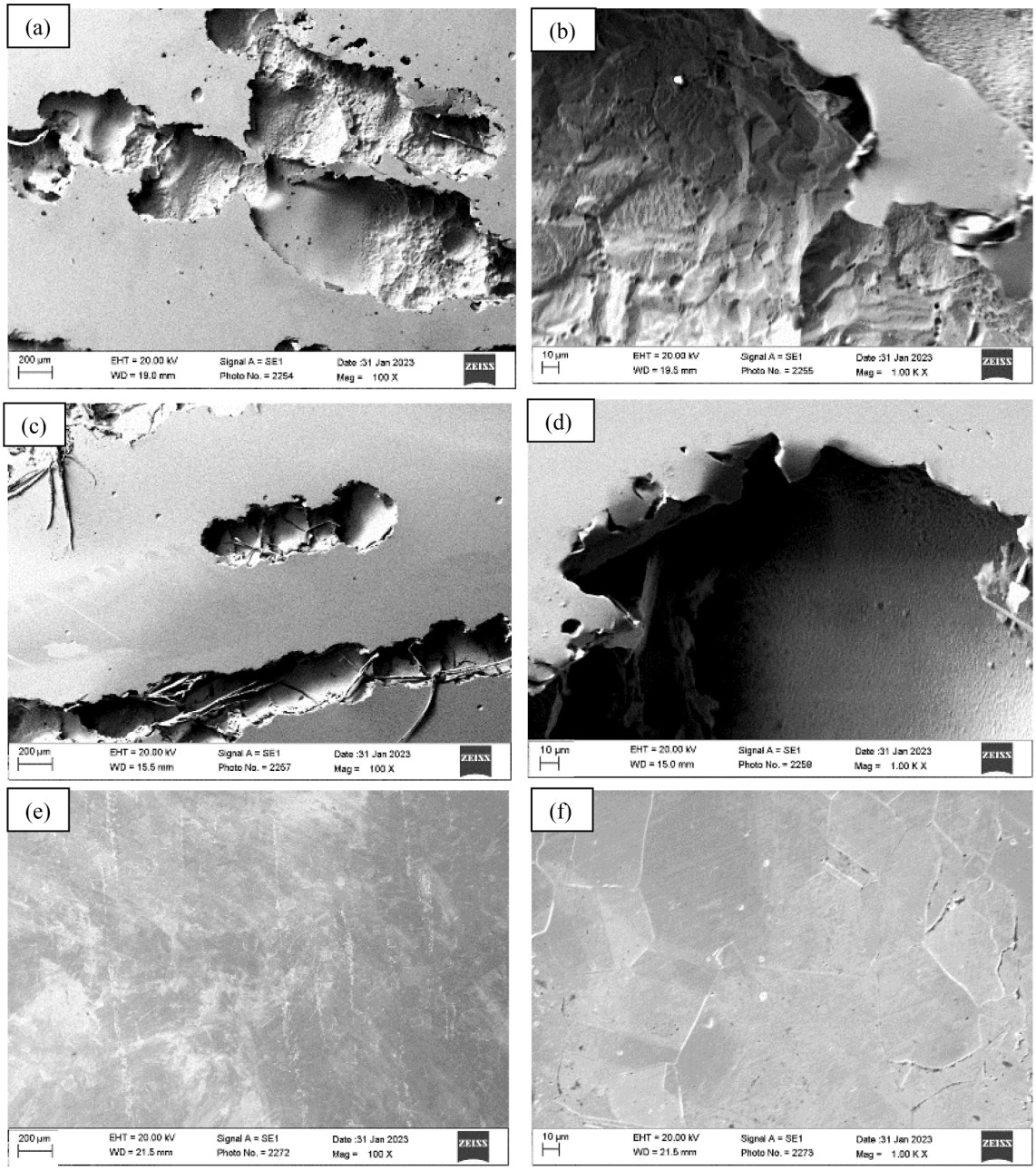

Fig. 10. SEM images (a) 304 NaCl, (b) 304 NH_4Cl, (c) 316L NaCl, (d) 316L NH_4Cl, (e) 317L NaCl and (f) 317L NH_4Cl.

pits in the austenitic 304 and 316L stainless steel samples are therefore susceptible to these electrolytes. In corrosion tests, pits usually appear morphologically as a circular or elliptical cavity on the surface of stainless steel [130]. It is noteworthy that pitting can be observed as a depression on the surface of stainless steel, penetrating towards the internal structure of the material. Pit depth can vary from a few micrometers to thousands of micrometers, depending on the corrosion conditions [131,132]. The pit may have jagged and rough edges, indicating progressive corrosion of the material around the pit. Based on the images, it can be seen that the austenitic 317L stainless steel has a high resistance to the media tested in this paper.

5. Discussion

A variety of corrosive substances can promote corrosion in equipment in oil refineries, including ammonia, carbon dioxide, chlorides, cyanides, hydrogen, naphthenic acids, oxygen, phenols, sulfuric acid, polythionic acids, acidic waters, washing waters, oil, hydrogen sulfide. Corrosion is currently considered the main form of damage mechanism in the oil refining industry, and the search for methodologies that identify it in advance, and that can safely predict the physical state of the equipment, part of this solution is part of the development of research that promotes the expansion of the tools available today for the evaluation of structural integrity in equipment.

The study of the corrosive process in metallic materials exposed to petroleum or its derived products, becomes extremely relevant, as it makes it possible to understand the isolated and / or synergistic action between various types and forms of corrosion that end up promoting degradation in metallic materials, in addition to avoiding or minimizing various problems of loss of contingency of systems and equipment, environmental damage, loss of loss of profit, economic losses and human losses.

It is important to highlight the corrosive action of ammonium chloride, which mainly attacks heat exchangers, pressure vessels and pipes of gasoline and diesel hydrotreating units. These units generally aim to remove sulfur and nitrogen as hydrogen sulfide and ammonia, respectively. In addition to hydrodesulphurization and hydrodenitrogenation functions, aromatics saturation reactions (hydrodesulphurization) are responsible for density reduction (diesel volumetric expansion) and increase of its cetane number. The reliability of these units has become essential for the continued operation of refineries.

High chloride in the load of the hydrotreatment units can result in salt formation and fouling in the exchangers that cool the reactor effluent, in a region of the battery where there is usually no facility for injecting wash water. Another point of attention is the corrosiveness of chloride to stainless steel, a material commonly used in these heat exchangers.

Corrosion caused by ammonium chloride is an electrochemical process that occurs due to the presence of the chloride ion (Cl^-) in the compound. The chloride ion is an aggressive agent that can attack many types of metals, especially those that are more susceptible to corrosion, such as iron and carbon steel, even stainless steels are susceptible to this type of corrosion.

When ammonium chloride comes into contact with a metal, the formation of an aqueous solution containing chloride ions occurs. These ions can react with the surface of the metal, causing corrosion. The electrochemical reaction usually involves the oxidation of the metal, where the metal ions are converted into positively charged metal ions (cations) and release electrons. The presence of ammonium chloride increases the rate of corrosion as chloride ions facilitate the transport of electrons in the solution, accelerating oxidation reactions in the metal. In addition, corrosion can also be aggravated by the presence of moisture, as water is required to facilitate the chemical reactions involved in the corrosive process.

It is noted that ammonium chloride corrosion is a type of general or localized corrosion, often in the form of pitting corrosion, normally occurring in the form of ammonium chloride or amine salt deposits, often in the absence of a free water phase. Ammonium chloride salts are hygroscopic and absorb water rapidly. A small amount of water can usually lead to very aggressive corrosion. Ammonium chloride corrosion is typically very localized and results in pitting corrosion, and corrosion rates can be extremely high.

Pitting corrosion, also known as “pitting corrosion,” is a type of localized corrosion that can occur in austenitic stainless steels in aqueous solutions containing sodium chloride (NaCl) or other chloride ions. The formation mechanism of this type of corrosion involves a number of phases:

Initiation phase: Pitting corrosion begins with the formation of small, corroded areas called “pites”. These areas can be triggered by various factors, including impurity inclusions on the surface of the stainless steel, micro-cracks, imperfections, or defects in the passivation, which is a thin layer of oxide that normally protects stainless steel from corrosion.

Chloride accumulation phase: Chloride ions (Cl^-) in aqueous solution play a fundamental role in this type of corrosion. They have an affinity for concentrating in areas where passivation has been compromised, such as the aforementioned imperfections. This leads to the accumulation of chloride in the damaged areas. Ion concentration phase (H^+): The accumulation of chloride in the affected areas lowers the local pH of the solution. As a result, the concentration of H^+ ions increase in these areas. This localized acidic environment is very corrosive for stainless steel.

Anodic corrosion phase: In the areas where pits form, the stainless steel undergoes anodic corrosion. This means that the iron atoms in the metallic structure of the steel lose electrons, forming iron ions (Fe^{+2}). These iron ions are released into solution. Cathodic corrosion phase: In order to maintain electroneutrality, anodic corrosion in the pitting areas must be accompanied by a cathodic reaction. This reaction takes place in areas adjacent to the pitting, where oxygen dissolved in the solution captures the electrons released in the anodic reaction, forming hydroxyl ions (OH^-).

Pitting growth phase: With the continuous loss of iron ions in the corroded areas and the formation of adjacent hydroxyl ions, the pitting begins to grow in depth and diameter. This leads to the formation of small cavities on the surface of the stainless steel.

Localized destruction phase: As the pites grow, they can penetrate deeper into the material, compromising its structural integrity. Pitting corrosion is especially dangerous because it can be highly localized, resulting in sudden and unpredictable failure of structures.

The formation mechanism of pitting corrosion in a medium containing ammonium chloride is very similar to that presented in

sodium chloride, but there are some significant differences, such as the addition of the following two phases:

Ammonia (NH_3) formation phase: NH_4Cl also releases ammonium ions (NH_4^+) into the solution. In high pH (alkaline) environments, the ammonium ion is converted into ammonia (NH_3). The formation of ammonia contributes to an increase in local pH in the affected areas.

Local alkaline pH increase phase: The presence of ammonia (NH_3) leads to an increase in local pH in the areas where pitting corrosion is occurring. This localized alkaline environment is less corrosive to stainless steel than an acidic environment, such as that observed in pitting corrosion in solutions containing sodium chloride (NaCl).

Electrochemical techniques are widely used for fundamental corrosion studies as they offer tools for studying corrosion mechanisms and provide data on the kinetics of corrosion reactions more quickly than traditional gravimetric techniques. The application of electrochemical corrosion techniques can provide a rapid response to the real behavior of the industrial plant in the face of adverse operating conditions and the influence of corrosive processes.

The type of salt formed in the high-pressure section of the hydrorefining units is associated with the contaminants present in the charge and or hydrogen replacement gas stream. Additives used in oil streams as neutralizers can add traces of nitrogen compounds. Both gaseous contaminants may combine to form the salt ammonium chloride. Some cargoes may also contain halogen-based compounds (bromine, chlorine, and fluorine), which in the presence of NH_3 may form the respective ammonium halides (NH_4Br, NH_4Cl and NH_4F). Hydrogen from the catalytic reforming process may contain HCl.

Despite these significant concerns, industry knowledge of aqueous ammonium chloride corrosion is still very limited. Ammonium chloride is considered an acid salt because it is formed by a strong acid (HCl) and a weak base (NH_3). Dilute solutions of stoichiometric NH_4Cl salt (less than 0.1 % by weight) are generally not considered very corrosive. However, corrosion is most severe at or near the aqueous dew point, where the NH_4Cl concentration can be very high.

6. Conclusions and preventive action

This study successfully investigated the failure that occurred in a load preheater heat exchanger shell and tubes of a diesel hydrotreating unit in a Brazilian refinery in the first half of 2022, where it was found that ammonium chloride (NH_4Cl) corrosion was the root cause of the observed damage.

Using electrochemical techniques in stainless material samples as an alternative to carbon steel, it was observed that the tested austenitic 317L stainless-steel samples in NH_4Cl solutions, compared to 304 and 316L, present characteristics of high passivation regions, higher values of potential pit formation (+0.470 V), reduced passivation current density values (4.426×10^{-8} A cm^{-2}), lower corrosion rate values (1.163×10^{-4} mm ano^{-1}) and higher impedance values, with capacitance (1.919×10^{-4} Farad) and polarization resistance (9.815×10^{4} Ohm). This behavior is due to the addition of the molybdenum alloying element in its composition, which increases its resistance to corrosion, mainly the form of localized corrosion. In general, the austenitic 317L stainless steel was more resistant to corrosive attacks in media containing sodium and ammonium chloride, which synthesizes several petroleum refining processes, including mainly gasoline and diesel hydrotreating units.

For both electrochemical measurement techniques used in this paper (potentiodynamic polarization and electrochemical impedance spectroscopy), the material 317L austenitic stainless steel was shown to have the highest resistance to localized corrosion among the materials analyzed. In sequence, in the corrosion resistance capacity, there are the 316L and 304L stainless steels. Therefore, 317L steel is to be specified in the design, construction and assembly stage of equipment, pipes and ducts that work in processes in which ammonium chloride presents itself as an active damage mechanism, such as that observed in petrochemical plants. The application of this steel will enable potential gains in terms of extending the operational life of equipment and facilities, reducing interventions for corrective maintenance, reducing the disposal of waste from processing units for corrective action, operational safety for oil refinery operators, in addition to increasing reliability throughout the period of operation of the industrial plant.

The choice of mitigation solutions depends on the specific conditions of the refinery, the materials used, ammonium chloride concentrations and local regulations. A comprehensive asset integrity management program is essential to identify, evaluate and implement the most appropriate strategies to prevent and mitigate ammonium chloride corrosion. In addition, we also recommend mitigating and preventive actions against ammonium chloride corrosion, adopting controlling and monitoring processes of the chemical composition load of hydrotreating units, measures such as protective coatings, surface treatments, use of corrosion-resistant materials can be adopted, implementing a washing water system using a dispersing nozzle, avoiding the unit design phase, the presence of regions without drainage, called the dead section, and as analyzed in this work, adopting austenitic 317L stainless steel in equipment and tubes that operate with loads containing ammonium chloride. But even the most corrosion-resistant nickel-based alloys and titanium alloys can undergo pitting corrosion in ammonium chloride.

Declaration of Competing Interest

The authors declare that they have no known competing financial interests or personal relationships that could have appeared to influence the work reported in this paper.

Data availability

The data that has been used is confidential.

Acknowledgements

Authors are grateful to the support from the Petrobras Regap the Brazilian oil refinery and Federal Center for Technological Education of Minas Gerais, through the Post-Graduate Program in Materials Engineering. This study was financed in part by the Coordination for the Improvement of Higher Education Personnel – Brazil (CAPES) – Finance Code 001.

References

[1] Y.T. Al-Janabi, An overview of corrosion in oil and gas industry, upstream, midstream, and downstream sectors (1) (2020). https://doi.org/10.1002/9783527822140.
[2] A. Grovsman, Corrosion control at oil refinery units, Corrosion Problems and Solutions in Oil Refining and Petrochemical Industry 32 (2017), https://doi.org/10.1007/978-3-319-45256-2_8.
[3] A. Groysman, Corros. Probl. Solut Oil Refining Petrochem. Ind. 32 (1) (2017) 356p, https://doi.org/10.1007/978-3-319-45256-2.
[4] J.D. Harston, F. ropital, Corrosion in refinery units, Woodhead Publishing in Materials 1 (2014), https://doi.org/10.1016/j.jscs.2021.101370.
[5] A.H. Al-Moubaraki, I.B. Obot, Corrosion challenges in petroleum refinery operations: sources, mechanisms, mitigation, and future Outlook, J. Saudi Chem. Soc. 25 (2) (2021) 101–370, https://doi.org/10.1016/j.jscs.2021.101370.
[6] S.A. Treese, The origins and fates of chlorides in hydroprocessing units, Digital Refining 3 (2019) 57–65.
[7] J.G. Speight, Handbook of petroleum product analysis, 2. ed, John Wiley & Sons, New Jersey, 2015.
[8] API RP-571, Damage mechanisms affecting fixed equipment in the refining and petrochemical industries, American Petroleum Institute, (3) (2020) 376p.
[9] API RP-932-A, A study of corrosion in hydroprocess reactor effluent air cooler systems, American Petroleum Institute, (1) (2002) 64p.
[10] G. Ou, Y. Gu, C. Yu, H. Jin, Failure analysis of ammonium chloride salt coagulation corrosion of U-tube heat exchanger in diesel hydrogenation unit, Eng. Fail. Anal. 137 (2022) 106–264, https://doi.org/10.1016/j.engfailanal.2022.106264.
[11] K. Toba, T. Suzuki, K. Kawano, J. Sakai, Effect of relative humidity on ammonium chloride corrosion in refineries, Corrosion 67 (5) (2011), https://doi.org/10.5006/1.3590331.
[12] C. Subramanian, D. Ghosh, D.S. Reddy, D. Ghosh, R. Natarajan, S.P. Velavan, Stress corrosion cracking of U tube heat exchanger used for low pressure steam generation in a hydrogen unit of petroleum refinery, Eng. Fail. Anal. 137 (2022) 106–245, https://doi.org/10.1016/j.engfailanal.2022.106245.
[13] K. Ravindranath, R. Alazemi, Failure of stainless steel 304L air cooler tubes due to stress corrosion cracking caused by organic chlorides, Eng. Fail. Anal. 102 (2019) 79–86, https://doi.org/10.1016/j.engfailanal.2019.04.029.
[14] S. Wang, S. Xu, S. Huang, Failure analysis of authentic stainless steel tubes in a vertical fixed shell–tube heat exchanger, J Fail. Anal. Preven. 18 (2018) 405–412, https://doi.org/10.1007/s11668-018-0423-7.
[15] M. Ali, A. Ul-Hamid, L.M. Alhems, A. Saeed, Review of common failures in heat exchangers – Part I: Mechanical and elevated temperature failures, Eng. Fail. Anal. 109 (2020) 104–396, https://doi.org/10.1016/j.engfailanal.2020.104396.
[16] D. Liu, J. Hu, X. Juan, L. Zhou, X. Zhong, Failure analysis and experimental verification on the hydrogen-driven pitting corrosion of heat exchanger tube material, Eng. Fail. Anal. 137 (2022) 106–283, https://doi.org/10.1016/j.engfailanal.2022.106283.
[17] K.V. Akpanyung, R.T. Loto, M.A. Fajobi, An overview of ammonium Chloride (NH4Cl) corrosion in the refining unit, J. Physics: Conference Series 1378 (2) (2019) 022–089, https://doi.org/10.1088/1742-6596/1378/2/022089.
[18] S. Mahajanam, F. Addington, A. Barba, B. Copple, N. Cuenca, J. Folse, Y. Mao, J. White, K. Williamson, Ammonium Chloride Corrosion in the Refining Industry, Corrosion NACE-2017-9574 (2017). 125-662.
[19] O. Forse, J. Aromma, M. Tavi, Corrosion resistance of different materials in dilute ammonium chloride-bearing environments, Corros. Sci. 35 (4) (1993) 297–301, https://doi.org/10.1016/0010-938X(93)90161-9.
[20] A.R. Brooks, C.R. Clayton, K. Doss, Y.C. Lu, On the role of cr in the passivity of stainless steel, J Elec Soc 133 (1986) 024–059, https://doi.org/10.1149/1.2108450.
[21] H. Tong, X. Liu, Y. Sui, F. Liu, Y. Liu, X. Li, J. Hou, Failure analysis of 70/30 cupronickel tubes serving in a heat exchanger, Eng. Fail. Anal. 152 (2023) 107–460, https://doi.org/10.1016/j.engfailanal.2023.107460.
[22] R.K. Pandey, Failure analysis of refinery tubes of overhead condenser, Eng. Fail. Anal. 13 (2006) 739–746, https://doi.org/10.1016/j.engfailanal.2005.02.016.
[23] H. Panahi, A. Eslami, M.A. Golozar, A.A. Laleh, An investigation on corrosion failure of a shell-and-tube heat exchanger in a natural gas treating plant, Eng. Fail. Anal. 118 (2020) 104–918, https://doi.org/10.1016/j.engfailanal.2020.104918.
[24] R.T. Mousavian, E. Hajjari, D. Ghasemi, M.K. Maneshc, K. Ranjbar, Failure analysis of a shell and tube oil cooler, Eng. Fail. Anal. 18 (2011) 202–211. https://doi.org/10.1016/j.engfailanal.2010.08.022.
[25] S.R. Allahkaram, P. Zakersafaee, S.A.M. Haghgoo, Failure analysis of heat exchanger tubes of four gas coolers, Eng. Fail. Anal. 18 (2011) 1108–1114. https://doi.org/10.1016/j.engfailanal.2010.11.015.
[26] S. Liu, H. Wu, Q. Zhao, Z. Liang, Corrosion failure analysis of the heat exchanger in a hot water heating boiler, Eng. Fail. Anal. 142 (2022) 106–847, https://doi.org/10.1016/j.engfailanal.2022.106847.
[27] D. Liu, H. Junying, X. Yuan, L. Zhou, X. Zhong, Failure analysis and experimental verification on the hydrogen-driven pitting corrosion of heat exchanger tube material, Eng. Fail. Anal. 137 (2022) 106–283, https://doi.org/10.1016/j.engfailanal.2022.106283.
[28] H.B. Wang, Y. Li, G.X. Cheng, W. Wu, Y.H. Zhang, X.Y. Li, Electrochemical investigation of corrosion of mild steel in NH4Cl solution, Int. J. Electrochem. Sci. 13 (2018) 5268–5283. https://doi.org/10.20964/2018.06.05.
[29] J.L. Hudson, T.T. Tsotsis, Electrochemical reaction dynamics: a review, Chem. Eng. Sci. 49 (10) (1994) 1493–1572.
[30] J.A.P. Nicacio, A.Q. Bracarense, V.F.C. Lins, Failure analysis in heat exchanger tubes from the top system of the regeneration tower of the hydrotreatment unit in an oil refinery: a case study, Revista Materia 26 (03) (2022) 30–35, https://doi.org/10.1590/S1517-707620210003.13035.
[31] J.A.P. Nicacio, A.Q. Bracarense, V.F.C. Lins, Failure analysis in heat exchanger tubes from the top system of the regeneration tower of the hydrotreatment unit in an oil refinery: a case study, Revista Materia 26 (3) (2021) 12p, https://doi.org/10.1590/S1517-707620210003.13035.
[32] H. Lin, H. Lagad, Evaluating Ammonium Chloride Corrosion Potential with Water Partial Pressure. NACE-8960, Corrosion (2017) 26-30.
[33] X. Liu, A. Duan, J. Quan, et al., A study on the corrosion failure induced by the ammonium chloride deposition in a high-pressure air cooler system, Eng. Fail. Anal. 112 (2020) 104–529, https://doi.org/10.1016/j.engfailanal.2020.104529.
[34] H.A. Al-Mazeedi, B. Al-Wakaa, K. Ravindranath, Window-type rupture of carbon steel pipe in a hydroprocessing plant of a petroleum refinery due to ammonium bisulfide corrosion, Eng. Fail. Anal. 120 (2021) 089–105, https://doi.org/10.1016/j.engfailanal.2020.105089.
[35] D. Liu, J. Hu, X. Yuan, et al., Failure analysis and experimental verification on the hydrogen-driven pitting corrosion of heat exchanger tube material, Eng. Fail. Anal. 137 (2022) 106–283, https://doi.org/10.1016/j.engfailanal.2022.106283.
[36] X. Liu, H. Zhu, C. Yu, et al., Analysis on the corrosion failure of U-tube heat exchanger in hydrogenation unit, Eng. Fail. Anal. 125 (2021) 105–448, https://doi.org/10.1016/j.engfailanal.2021.105448.
[37] I.B. Obot, A.A. Sorour, C. Verma, et al., Key parameters affecting sweet and sour corrosion: Impact on corrosion risk assessment and inhibition, Eng. Fail. Anal. 145 (2023) 008–107, https://doi.org/10.1016/j.engfailanal.2022.107008.
[38] H. Jin, X. Chen, G. Ou, et al., Potential failure analysis and prediction of multiphase flow corrosion thinning behavior in the reaction effluent air cooler system, Eng. Fail. Anal. 109 (2020) 104–274, https://doi.org/10.1016/j.engfailanal.2019.104274.
[39] Z. Yan, L. Wang, P. Zhang, et al., Failure analysis of erosion-corrosion of the bend pipe at sewage stripping units, Eng. Fail. Anal. 129 (2021) 105–675, https://doi.org/10.1016/j.engfailanal.2021.105675.

[40] Z. Zhenga, G. Oua, H. Ye, et al., Analysis on the under-deposit corrosion of air cooler tubes: thermodynamic, numerical, and experimental study, Eng. Fail. Anal. 79 (2017) 726–736, https://doi.org/10.1016/j.engfailanal.2017.05.018.
[41] G. Ou, H. Jin, H. Xie, et al., Prediction of ammonium salt deposition in hydroprocessing air cooler tubes, Eng. Fail. Anal. 18 (2011) 1458–1464, https://doi.org/10.1016/j.engfailanal.2011.04.011.
[42] H. Jin, X. Chen, Z. Zheng, et al., Failure analysis of multiphase flow corrosion–erosion with three-way injecting water pipe, Eng. Fail. Anal. 73 (2017) 46–56, https://doi.org/10.1016/j.engfailanal.2016.12.005.
[43] A.H. Alamri, Localized corrosion and mitigation approach of steel materials used in oil and gas pipelines – an overview, Eng. Fail. Anal. 116 (2020) 104–735, https://doi.org/10.1016/j.engfailanal.2020.104735.
[44] P.P. Alvisi, V.F.C. Lins, Acid salt corrosion in a hydrotreatment plant of a petroleum refinery, Eng. Fail. Anal. 15 (2008) 1035–1041. https://doi.org/10.1016/j.engfailanal.2007.11.014.
[45] L. Sun, M. Zhu, G. Ou, Corrosion investigation of the inlet section of REAC pipes in the refinery, Eng. Fail. Anal. 66 (2016) 468–478, https://doi.org/10.1016/j.engfailanal.2016.05.009.
[46] M. Zhu, L. Sun, G. Ou, et al., Erosion corrosion failure analysis of the elbow in sour water stripper overhead condensing reflux system, Eng. Fail. Anal. 62 (2016) 93–102, https://doi.org/10.1016/j.engfailanal.2016.01.002.
[47] Z. Zheng, G. Ou, H. Ye, Investigation on the deposition failure of a reactor effluent air cooler in hydrocracking unit, Eng. Fail. Anal. 68 (2016) 52–63, https://doi.org/10.1016/j.engfailanal.2016.05.005.
[48] G. Ou, K. Wang, J. Zhan, et al., Failure analysis of a reactor effluent air cooler, Eng. Fail. Anal. 31 (2013) 387–393, https://doi.org/10.1016/j.engfailanal.2013.02.025.
[49] R. Li, H. Huang, X. Wang, Y. Wang, Effect of ammonium salt on corrosion of pipelines and components in a crude oil distillation column: Electrochemical and AIMD studies, Corros. Sci. 203 (2022) 110–362, https://doi.org/10.1016/j.corsci.2022.110362.
[50] K. Toba, T. Uegaki, T. Asotani, A New Approach to Prevent Corrosion of the Reactor Effluent System in HDS Units, paper 3653, Corrosion (2003) (NACE).
[51] API RP-932-B, Design, materials, fabrication, operation, and inspection guidelines for corrosion control in hydroprocessing reactor effluent air cooler (REAC) system, American Petroleum Institute, (3) (2019) 70p.
[52] A study of corrosion in hydroprocessing reactor effluent air cooler system (API RP 932-A) 2002 (NACE).
[53] A study of corrosion in hydroprocessing reactor effluent air cooler system (API RP 932-B) 2012 (NACE).
[54] A study of corrosion in hydroprocessing reactor effluent air cooler system (API RP 932-B) 2012 (NACE).
[55] A. Sun, D. Fan, Prediction, monitoring, and control of ammonium chloride corrosion in refining processes, paper 359, Corrosion 10 (2010). NACE.
[56] C. Shargay, J. Turner, et al., Design considerations to minimize ammonium chloride corrosion in hydrotreater REAC's, paper 543, Corrosion 01 (2001). NACE.
[57] H. Iwawaki, K. Toba, Corrosion behavior of steel in concentrated NH_4HS environments, paper 576, Corrosion 07 (2007) (NACE).
[58] R.J. Horvath, M.S. Cayard, R.d., Kane, prediction and assessment of ammonium bisulfide corrosion under refinery sour water service conditions, paper 576, Corrosion 06 (2006). NACE.
[59] K. Toba, T. Suzuki, K. Kawano, et al., Effect of relative humidity on ammonium chloride corrosion in refinery, Corrosion 67 (5) (2011) 13–21, https://doi.org/10.5006/1.3590331.
[60] Y.G. Zheng, B. Brown, S. Nesic, Electrochemical study and modeling of H_2S corrosion of mild steel, Corrosion 70 (4) (2014) 351–365, https://doi.org/10.5006/0937.
[61] M. Zhu, G. Ou, H. Jin, et al., Top of the REAC tube corrosion induced by under deposit corrosion of ammonium chloride and erosion corrosion, Eng. Fail. Anal. 57 (2015) 483–489, https://doi.org/10.1016/j.engfailanal.2015.08.022.
[62] G. Ou, Y. Gu, C. Yu, et al., Failure analysis of ammonium chloride salt coagulation corrosion of U-tube heat exchanger in diesel hydrogenation unit, Eng. Fail. Anal. 137 (2022) 106–264, https://doi.org/10.1016/j.engfailanal.2022.106264.
[63] V. Cruz, Q. Chao, N. Birbilis, et al., Electrochemical Studies on the effect of residual stress on the corrosion of 316L manufactured by seletive laser melting, Corros. Sci. 164 (2020) 108–314, https://doi.org/10.1016/j.corsci.2019.108314.
[64] D. Macdonald, Reflections on the history of electrochemical impedance spectroscopy, Electrochim. Acta 51 (20) (2006) 1376–1388, https://doi.org/10.1016/j.electacta.2005.02.107.
[65] M. Esser, G. Rohde, C. Rehtanz, Electrochemical impedance spectroscopy setup based on standard measurement equipment, J. Power Sources 544 (2022) 231–869, https://doi.org/10.1016/j.jpowsour.2022.231869.
[66] J. Gao, Y. Jiang, B.o. Deng, et al., Investigation of selective corrosion resistance of aged lean duplex stainless steel. Nondestructive electrochemical techniques, Electrochim. Acta 54 (24) (2009) 5830–5835, https://doi.org/10.1016/j.electacta.2009.05.039.
[67] K. Kano, S. Hagiwara, T. Igarashi, et al., GIRISHA, K. G. et al. Study on the free corrosion potential at an-interface between an Al electrode and an acidic aqueous NaCl solution through density functional theory combined with the reference interaction site model. Electrochimica Acta, 377 (2021) 121-138. https://doi.org/10.1016/j.electacta.2021.138121.
[68] M. Gomes, S. Gateman, I. Gomes, et al., Improved experimental setup to reach a broad frequency domain in local electrochemical impedance spectroscopy measurements, Measurement 200 (2022) 111–504, https://doi.org/10.1016/j.measurement.2022.111504.
[69] H. Hernández, A. Reynoso, J. González, et al. Electrochemical impedance spectroscopy (EIS): a review study of basic aspects of the corrosion mechanism applied to steels, In Web of Science Core Collection, IntechOpen, (2020) 36p. https://doi.org/10.5772/intechopen.94470.
[70] J.Z. Jun, C. Du, C. Li, et al., Study on pitting process of 316L stainless steel by means of staircase potential electrochemical impedance spectroscopy, Int. J. Miner. Metall. Mater. 18 (1) (2011) 48–54, https://doi.org/10.1007/s12613-011-0398-9.
[71] K. Kano, S. Hagiwara, T. Igarashi, et al., Study on the free corrosion potential at an interface between an Al electrode and an acidic aqueous NaCl solution through density functional theory combined with the reference interaction site model, Electrochim. Acta 377 (2021) 121–138, https://doi.org/10.1016/j.electacta.2021.138121.
[72] A. Lasia, Electrochemical Impedance Spectroscopy and its Applications, New York: Editora Springer (1) (2014) 367p. .
[73] H.A. Al-Mazeedi, A. Al-Farhan, N. Tanoli, et al., A study of galvanic corrosion in stagnant ammonium bisulfide solution, Int. J. Corros. (2019) 9p, https://doi.org/10.1155/2019/1325169.
[74] H.A. Al-Mazeedi, A. Al-Farhan, N. Tanoli, et al., A Study of galvanic corrosion in flowing ammonium bisulfide solution, J. Geol. Geosci. 3 (1) (2018) 9p, https://doi.org/10.1155/2019/1325169.
[75] A. Pardo, M.C. Merino, A.E. Coy, et al., Pitting corrosion behaviour of austenitic stainless steels – combining effects of Mn and Mo additions, Corros. Sci. 50 (6) (2008) 1796–1806, https://doi.org/10.1016/j.corsci.2008.04.005.
[76] R. Jiang, Y. Wang, X. Wen, et al., Effect of time on the characteristics of passive film formed on stainless steel, Appl. Surf. Sci. 412 (2017) 214–222, https://doi.org/10.1016/j.apsusc.2017.03.155.
[77] ASTM G967-17, Standard specification for chemical passivation treatments for stainless steel parts, 01.03, (2017). https://doi.org/10.1520/A0967_A0967M-17.
[78] ASTM E797-21, Standard practice for measuring thickness by manual ultrasonic pulse-echo contact method, American Society for Testing and Materials, 03.03, (2021). https://doi.org/10.1520/E0797_E0797M-21.
[79] ASTM G1-03, Standard practice for preparing, cleaning, and evaluating corrosion test specimens, American Society for Testing and Materials, 03.02, (2017). https://doi.org/10.1520/G0001-03R17E01.
[80] ASTM A179-19, Standard specification for seamless cold-drawn low-carbon steel heat-exchanger and condenser tubes, American Society for Testing and Materials, 01.01, (2019). https://doi.org/10.1520/A0179_A0179M-19.
[81] NACE. Science of Pitting Corrosion, Corrosion Journal, National Association of Corrosion Engineers, 70 (2014) 781p.
[82] V. Maurice, H. Peng, L. Klain, et al., Effects of molybdenum on the composition and nanoscale morphology of passivated austenitic stainless steel surfaces, J Faraday Discuss. 180 (2015) 151–170, https://doi.org/10.1039/C4FD00231H.

[83] Astm g106–89,, Standard practice for verification of algorithm and equipment for electrochemical impedance measurements, Am Soc Test Mater 03 (02) (2015), https://doi.org/10.1520/G0106-89R15.
[84] ABNT NBR-ISO 12667-14, Chemical analysis of refractory products by X-ray fluorescence (XRF) — Fused cast bead method, 84 p., 2014. https://www.abntcatalogo.com.br/pnm.aspx?ID=4274.
[85] Z. Wang, S. Zanna, A. Seyeux, et al., Mechanisms of Cr and Mo enrichments in the passive oxide film on 316L austenitic stainless steel, Env. Deg. Mat. 6 (2019) 232–243, https://doi.org/10.3389/fmats.2019.00232.
[86] R.F. Guimarães, N.C. Figueiredo, V.M. Pinheiro, et al., Effect of the content of molybdenum in the microstructure of Fe-9Cr-xMo alloy, Revista Soldagem & Inspeção 15 (4) (2010), https://doi.org/10.1590/S0104-92242010000400002.
[87] J.A. Sedriks, Effect of alloy composition and microstruture on the passivity of stainless steel, Corrosion 42 (7) (1986) 376–389, https://doi.org/10.5006/1.3584918.
[88] G. Tranchida, M. Clesi, F. Franco, et al., Electronic properties and corrosion resistance of passive films on austenitic and duplex stainless steels, Electrochim. Acta 273 (2018) 412–423, https://doi.org/10.1016/j.electacta.2018.04.058.
[89] R. Aslam, Potentiodynamic polarization methods for corrosion measurement, Electrochem. Anal. Tech. Sustain. Corros. Monit. 01 (2023) 25–37, https://doi.org/10.1016/B978-0-443-15783-7.00003-7.
[90] H.J. Flitt, D. Schweinsberg, Evaluation of corrosion rate from polarisation curves not exhibiting a Tafel region, Corros. Sci. 47 (2005) 3034–3052, https://doi.org/10.1016/j.corsci.2005.06.014.
[91] X.L. Zhang, Z.H. Jiang, Z.P. Yao, Y. Song, Z.D. Wu, Effects of scan rate on the potentiodynamic polarization curve obtained to determine the Tafel slopes and corrosion current density, Corros. Sci. 51 (2009) 581–587, https://doi.org/10.1016/j.corsci.2008.12.005.
[92] Q. Liu, Q. Sun, S. Wang, K. Chen, Effect of scan rate on polarization curves of a high strength Al alloy in 3.5 wt% NaCl solution, Int. J. Electrochem. Sci. 16 (2021), https://doi.org/10.20964/2021.11.05.
[93] Z. Wang, S. Zanna, A. Seyeux, et al., Chloride-induced alterations of the passive film on 316L stainless steel and blocking effect of pre-passivation, Electrochim. Acta 329 (2020) 135–159, https://doi.org/10.1016/j.electacta.2019.135159.
[94] K.V. Akpanyung, R.T. Loto, Pitting corrosion evaluation: a review, J. Phys. Conf. Ser. 1378 (2) (2018) 22–88, https://doi.org/10.1088/1742-6596/1378/2/022088.
[95] ASTM A240-22a, Standard specification for chromium and chromium-nickel stainless steel plate, sheet, and strip for pressure vessels and for general applications, American Society for Testing and Materials, 01.03, (2022). https://doi.org/10.1520/A0240_A0240M-22A.
[96] I.A. Chaves, R.E. Melchers, Pitting corrosion in pipeline steel weld zones, Corros. Sci. 53 (12) (2011) 4026–4032, https://doi.org/10.1016/j.corsci.2011.08.005.
[97] G.T. Burstein, C. Liu, R.M. Souto, et al., Origins of pitting corrosion, the international journal of corrosion processes and corrosion, Control 39 (1) (2004) 25–30, https://doi.org/10.1179/147842204225016859.
[98] G.M. Tsoeunyane, E.M. Makhatha, Electrochemical and surface analytical study on the role of poly(butylene-succinate)-l-proline during corrosion of mild steel in 1 M HCl, Chemistry 2 (4) (2020) 900–917, https://doi.org/10.3390/chemistry2040057.
[99] ASTM E309-16, Standard practice for eddy-current examination of steel tubular products using magnetic saturation, American Society for Testing and Materials, 03.03, (2016). https://doi.org/10.1520/E0309-16.
[100] S. Sharma, R. Ganjoo, A. Thakur, A. Kumar, Electrochemical characterization, and surface morphology techniques for corrosion inhibition—a review, Chem. Eng. Commun. (2022) 1–36, https://doi.org/10.1080/00986445.2022.2039913.
[101] K. Yasakau, Application of AFM-based techniques in studies of corrosion and corrosion inhibition of metallic alloys, Corros. Mater. Degrad. 1 (3) (2020) 345–372, https://doi.org/10.3390/cmd1030017.
[102] T.E. Lister, P.J. Pinhero, The effect of localized electric fields on the detection of dissolved sulfur species from Type 304 stainless steel using scanning electrochemical microscopy, Elec-Trochim. Acta 48 (17) (2003) 2371–2378, https://doi.org/10.1016/S0013-4686(03)00228-7.
[103] S. Feliu, Electrochemical impedance spectroscopy for the measurement of the corrosion rate of magnesium alloys: brief review and challenges, Metals 10 (2020) 775, https://doi.org/10.3390/met10060775.
[104] A. Molhi, R. Hsissou, M. Damej, A. Berisha, M. Bamaarouf, M. Seydou, M. Benmessaoud, S. El Hajjaji, Performance of two epoxy resins against corrosion of C38 steel in 1M HCl: electrochemical, thermodynamic and theoretical assessment, Int. J. Corros. Scale Inhib. 10 (2) (2021) 812–837. https://doi.org/10.17675/2305-6894-2021-10-2-21.
[105] TEMA, Standards of Tubular Exchangers Manufactures Association, 9th Edn., New York, 2007.
[106] M. Schneider, on non-stationary polarisation methods in FFT-based computational micromechanics, Int. J. Numer. Meth. Eng. 122 (22) (2021), https://doi.org/10.1002/nme.6812.
[107] ASTM A213-06a, Standard Specification for Seamless Ferritic and Austenitic Alloy-Steel Boiler, Superheater, and Heat-Exchanger Tubes, American Society for Testing and Materials, 06a, (2006). https://doi.org/10.1520/a213a213m.
[108] P. Du, S. Deng, G. Du, D. Shao, D. Xu, X. Li, Synergistic inhibition effect of Mikania micrantha extract with potassium iodide on the corrosion of cold rolled steel in methanesulfonic acid solution, Corros. Sci. 220 (2023) 111–296, https://doi.org/10.1016/j.corsci.2023.111296.
[109] L. Zhou, Q. Zhao, G. Lv, Z. Dou, W. Um, T. Zhang, Effect of NH4Cl on the rusting leaching behavior of metallic phase of iron in reduced ilmenite during TiO2 purification: an electrochemical and density-functional theory study, Appl. Surf. Sci. 638 (2023), 158019, https://doi.org/10.1016/j.apsusc.2023.158019.
[110] P.K. Baranwal, P.V. Rajaraman, Electrochemical investigation on effect of sodium thiosulfate (Na2S2O3) and ammonium chloride (NH4Cl) on carbon steel corrosion, J. Mater. Res. Technology 8 (1) (2019) 1366–1378, https://doi.org/10.1016/j.jmrt.2018.05.029.
[111] F. Soleimangoli, S.A. Hosseini, A. Davoodi, A. Mokhtari, M. Alishahi, Effect of NH4Cl on the microstructure, wettability, and corrosion behavior of electrodeposited Ni–Zn coatings with hierarchical nano/microstructure, Surf. Coat. Technol. 394 (2020) 125–825, https://doi.org/10.1016/j.surfcoat.2020.125825.
[112] Q. Qu, L. Li, W. Bai, C. Yan, C. Cao, Effects of NaCl and NH4Cl on the initial atmospheric corrosion of zinc, Corros. Sci. 47 (2005) 2832–2840, https://doi.org/10.1016/j.corsci.2004.11.010.
[113] T. Bellezze, G. Giuliani, A. Viceré, G. Roventi, Study of stainless steels corrosion in a strong acid mixture. Part 2: anodic selective dissolution, weight loss and electrochemical impedance spectroscopy tests, Corros. Sci. 130 (2018) 12–21, https://doi.org/10.1016/j.corsci.2017.10.010.
[114] A.V. Vitaller, U.M. Angst, B. Elsener, A setup for electrochemical corrosion testing at elevated temperature and pressure, Measurement 155 (2020) 107–537, https://doi.org/10.1016/j.measurement.2020.107537.
[115] S. Mohammed, Y. Hua, R. Barker, A. Neville, Investigating pitting in X65 carbon steel using potentiostatic polarisation, Appl. Surf. Sci. 423 (2017) 25–32, https://doi.org/10.1016/j.apsusc.2017.06.015.
[116] R.K. Gupta, N.L. Sukiman, M.K. Cavanaugh, B.R.W. Hinton, C.R. Hutchinson, N. Birbilis, Metastable pitting characteristics of aluminium alloys measured using current transients during potentiostatic polarisation, Electrochim. Acta 66 (2012) 245–254, https://doi.org/10.1016/j.electacta.2012.01.090.
[117] J. Li, C.W. Du, Z.Y. Liu, X.G. Li, M. Liu, Effect of microstructure on the corrosion resistance of 2205 duplex stainless steel. Part 1: Microstructure evolution during isothermal aging at 850°C and evaluation of anticorrosion properties by methods of cyclic potentiodynamic polarization and electrochemical impedance tests, Constr. Build. Mater. 189 (2018) 1286–1293, https://doi.org/10.1016/j.conbuildmat.2018.08.186.
[118] Z.B. Saleh, A. Shahryari, S. Omanovic, Enhancement of corrosion resistance of a biomedical grade 316LVM stainless steel by potentiodynamic cyclic polarization, Thin Solid Films 515 (2007) 4727–4737, https://doi.org/10.1016/j.tsf.2006.11.054.
[119] B.M. Prasanth, E. Rajkeerthi, P. Hariharan, Polarization studies – a method to select and optimize electrolyte for electrochemical micromachining process, 06 (2023) 418-433.
[120] M. Zohoor, S. Jalili, A. Alipour, R. Mosallanejad, Effect of electrolyte type on electrochemical machining of 304 steel, Int. J. Adv. Eng. Res. 12 (2016) 20–39.
[121] M. Laleh, M. Pathirana, M.Y. Tan, Site-specific local polarisation curve measurements for probing localised corrosion and inhibition, 111-019, Corros. Sci. 214 (2023), https://doi.org/10.1016/j.corsci.2023.111019.

[122] D.D.S. Silva, J.M.B. Sobrinho, C.R. Souto, R.M. Gomes, Application of electromechanical impedance technique in the monitoring of sigma phase embrittlement in duplex stainless steel, Mater. Sci. Eng. 788 (2020) 139–457, https://doi.org/10.1016/j.msea.2020.139457.
[123] S. Feliu, J.C. Galvan, The application of electrochemical impedance spectroscopy to study the corrosion of magnesium alloys, Encyclopedia of Solid-Liquid, Interfaces 1 (2024) 550–564, https://doi.org/10.1016/B978-0-323-85669-0.00133-1.
[124] T. Tánski, W. Borek, M. Król, A Critical Review of the Application of Electrochemical Techniques for Studying Corrosion of Mg and Mg Alloys: Opportunities and Challenges, Magnes. Alloys Sel. Issue (2018) 694–738, https://doi.org/10.5772/intechopen.79497.
[125] F. Lisdat, D. Schäfer, The use of electrochemical impedance spectroscopy for biosensing, Anal. Bioanal. Chem. 391 (2008) 1555–1567, https://doi.org/10.1007/s00216-008-1970-7.
[126] A. Amirudin, D. Thierry, Application of electrochemical impedance spectroscopy to study the degradation of polymer-coated metals, Prog. Org. Coat. 26 (1995) 1–28.
[127] P. Mishra, D. Yavas, A. F. Bastawros, K. Hebert, Electrochemical impedance spectroscopy analysis of corrosion product layer formation on pipeline steel, Electrochimica Acta 346 (202) 136-232. https://doi.org/10.1016/j.electacta.2020.136232.
[128] R. Ke, L. Wang, Z. Zou, L. Zheng, Z. Sun, S. Lu, An analytical model for anchor-mortar interface bonding based on electrochemical impedance spectroscopy, Cem. Concr. Compos. 142 (2023) 105–196, https://doi.org/10.1016/j.cemconcomp.2023.105196.
[129] L.M. Baena, F.A. Vasquez, J.A. Calderón, Corrosion assessment of metals in bioethanol-gasoline blends using electrochemical impedance Spectroscopy, Heliyon 7 (2021) e07585.
[130] F. Sun, P. Han, B. He, An analysis of electrochemical corrosion on pipeline steel in silty soil under salt-temperature coupling environments, Chem. Eng. Science 274 (2023) 118–704, https://doi.org/10.1016/j.ces.2023.118704.
[131] C. Burkhardt, M. Wendler, R. Lehnert, M. Hauser, P. Clausnitzer, O. Volkova, H. Biermann, A. Weidner, Fine-grained microstructure without texture obtained by electron beam powder bed fusion for AISI 304 L-based stainless steel, Addit. Manuf. 69 (2023) 103–539, https://doi.org/10.1016/j.addma.2023.103539.
[132] S. Gao, C. Dong, H. Luo, K. Xiao, X. Pan, X. Li, Scanning electrochemical microscopy study on the electrochemical behavior of CrN film formed on 304 stainless steels by magnetron sputtering, Electrochim. Acta 114 (2013) 233–241, https://doi.org/10.1016/j.electacta.2013.01.009.